OULUN YLIOPISTO
UNIVERSITY of OULU

DEGREE PROGRAMME IN WIRELESS COMMUNICATIONS ENGINEERING

PERFORMANCE MEASUREMENTS OF DW1000 IMPLEMENTING IEEE STANDARD 802.15.4-2011 IMPULSE RADIO ULTRA WIDEBAND TECHNOLOGY

Thesis author _____
Ke Xu

Thesis supervisor _____
Dr. Jussi Haapola

Second examiner_____
Dr. Harri Posti

Approved _____/_____20

Grade _____

Abstract

This thesis is about testing a system's actual performance under the IEEE 802.15.4-2011 UWB specifications, with a compliant device DW1000. It is of great interest to test the synchronization ability of different preamble lengths, which are applied in the IEEE 802.15.4-2011 UWB standard. It is also urgent to know the system's actual performance in a multipath propagation environment, since the IEEE 802.15.4-2011 UWB standard allows an energy detection (ED) receiver to take advantage of multipath propagation.

Theory predicts that a long preamble length can offer better synchronization ability at long distances, and has a longer working range. On the other hand, a long preamble length requires a longer channel occupancy time and more power consumption. Thus, a long preamble may not be the optimal choice for working at short distances.

The channel model of the IEEE 802.15.4-2011 UWB standard, which is based upon the Saleh-Valenzuela (S-V) model, can be regarded as block fading. Although multipath propagation can improve the system's performance by increasing the SNR, the effects of block fading on the system must be taken into account as well. It is pointed out in various papers that the S-V model is precise in predicting a none-line-of-sight (NLOS) environment, while it is not precise in predicting a line-of-sight (LOS) environment.

The results of the first part of the measurements show that longer preambles have longer working ranges. However, the longer preambles' performance, in the term of the packet reception ratio, is not necessarily better than that of the shorter preambles.

The results of the second part of the measurements show that the system can take advantage of multipath propagation. On the other hand, the system's performance might become instable, due to block fading. The receiver and the transmitter will have difficulty in synchronization, if the channel impulse response changes too much within the unsynchronized time period. A longer preamble length tends to offer a longer stable working range. In addition, the path loss of the channel will suddenly increase and then decrease. This phenomenon of a sudden change in the path loss at a certain distance is quite similar to that of a narrowband system.

Key words: DW1000, IEEE 802.15.4-2011 UWB standard, preamble length, synchronization, multipath propagation, block fading, instable, S-V model, LOS.

Table of contents

Foreword

The aim of this thesis is to study the performance of the DW1000, under the IEEE 802.15.4-2011 UWB standard. It focuses on discussing how different preamble lengths could affect the system's performance in different scenarios. Measurements are needed in order to offer results, which can test the theory.

Several persons from the Department of Wireless Communication Engineering have taken part in setting up the measurements and supervising the thesis. Dr. Harri Posti led the whole topic. The supervisor of this thesis is Dr. Jussi Haapola. And Konstantin Mikhaylov had paid a lot of efforts in writing the software program for the measurements.

Oulu, Feb 12. 2016

Ke Xu

List of abbreviations and symbols

AC	Auto-correlation
ACK	Acknowledgement
ALOHA	Application layer optimization and high availability
BER	Bit error rate
BPAM	Binary pulse amplitude modulation
BPM/BPSK	Burst position modulation/binary phase shift keying
CIR_PWR	Channel impulse response power
CRC	Cyclic redundancy check
DS	Direct sequence
ED	Energy detection
FCE	Frame check sequence error
FCG	Frame check sequence good
FCS	Frame check sequence
FEC	Forward error control
FFR	Frame filter rejection
FWTO	Frame wait timeout
HPW	Half period warning
IR	Impulse radio
ISI	Inter-symbol interference
LFSR	Linear feedback shift register
LO	Local oscillator
LOS	Line-of-sight
LSB	Least significant bit

MAC	Multiple access control
MSB	Most significant bit
MPDU	MAC protocol data unit
MUI	Multi-user interference
NLOS	None-line-of-sight
OOK	On-off keying
OVR	Overrun
PAC	Preamble accumulation chunks
PAM	Pulse amplitude modulation
PHE	Physical header error
PHR	Physical header
PLCP	Physical layer convergence protocol
PLL	Phase locked loop
PG	Processing gain
PPDU	PLCP protocol data unit
PPM	Pulse position modulation
PR	Pseudo random
PRBS	Pseudo random binary sequence
PRF	Pulse repetition frequency
PSDU	PLCP service data unit
PSM	Pulse shape modulation
PTO	Preamble detection timeout
RF	Radio frequency
RS	Reed-Solomon
RSE	Reed-Solomon decoder error

SBY	Siwiak, Bertoni & Yano
SECDED	Single error correcting double error detecting
SFD	Start frame delimiter
SHR	Synchronization header
SK	Siwiak Kazimierz
SNR	Signal to noise ratio
STO	SFD timeout
S-V	Saleh-Valenzuela
TH	Time hopping
TPW	Transmitter power-up warning
TXFS	Transmitter frame sent
UWB	Ultra-wideband
WED	Weighted energy detection
d_p	Break point distance
f_H	High frequency
f_L	Low frequency
f_m	Mean frequency
$g_0^{(k)}$	Burst position bit
$g_1^{(k)}$	Burst polarity bit
$h^{(k)}$	Burst hopping sequence
N_s	Number of pulses per bit
N_U	Maximum number of non-overlapping users
R	Reflection coefficient
R_s	Symbol rate

T_c	Chip duration
T_f	Duration of the time hopping frame
T_p	Width of the pulse
T_s	Symbol duration time
$s_{n+kN_{cpb}}$	Chip scrambling sequence
γ	Magnitude of ground reflection coefficient
ε_r	Complex dielectric constant of the reflecting surface
φ	Phase of the reflection coefficient

1. Introduction

This chapter gives an overall introduction on the entire thesis. Nowadays, more and more researches have made studies how the ultra-wideband (UWB) technology can be applied for commercial use, especially data communication. The application of the UWB for data communication has become a hot topic since 2002 [1].

There are varieties of uses for the UWB technology. According to [37], the UWB technology can be used for radio frequency identification (RFID). The use of the UWB in the medical domain has also become a hot topic [35, 40]. According to [36], the UWB can be used in the wireless body area networks. The UWB can also be used for localization in wireless sensor networks [39]. On the other hand, the localization ability of the UWB technology has limitations, in the term of precision [44]. Precise three dimensional imaging of complex objects can be achieved by using the UWB technology [41, 42]. Moreover, the UWB technology is being applied in the near-field imaging, where taking the image of individual atoms on the surface of materials becomes possible [43].

Plentiful studies have been done to give theoretical predictions on the performance of the IEEE 802.15.4-2011 UWB standard. The DW1000 is a production device, which is compliant with the IEEE 802.15.4-2011 UWB specifications. The DW1000 is considered to be of low cost and complexity [7].

The IEEE 802.15.4-2011 UWB standard has its unique preamble sequence, which is used for synchronization [5]. The synchronization ability of a preamble sequence is dependent on its length [14]. Although some theoretical predictions on the synchronization ability of a preamble sequence with different lengths have been made, it is of great interest to test its actual synchronization ability with a compliant device. Moreover, the IEEE 802.15.4-2011 UWB standard is known to have the ability to take advantage of multipath propagation [1]. Thus, it is also necessary to test the system's actual performance in a multipath propagation environment.

The topic of this thesis is to study the actual performance of the IEEE 802.15.4-2011 UWB system, by using the DW1000 hardware device. It mainly focuses on finding out how different preamble lengths can affect the synchronization ability of the system. In addition, how multipath propagation can affect the system's performance is tested as well. The results of the test can also show the DW1000's performance. In order to fulfill the test, two parts of measurements will be carried out.

The first part of measurements will focus on testing the performance of different preamble lengths in an environment, with minimal multipath components. The results show the natural synchronization abilities of different preamble lengths, and how they will affect the system's performance.

The second part of measurements will focus on finding out how differently the system will perform in an environment with multipath propagation. The results of this part will show the effects of multipath propagation on the system's performance. Moreover, the results can also show how the multipath propagation affects the synchronization abilities of the different preamble lengths.

The second chapter of this thesis will introduce the basic concepts of UWB and the IEEE 802.15.4-2011 UWB specifications. The second chapter will mainly focus on introducing the physical structure of the IEEE 802.15.4-2011 UWB standard. Different channel models will also be discussed, in order to analyze the environments of the measurements.

The third chapter of this thesis will introduce the measurements' settings. First, the necessary functionalities and the operational process will be introduced in detail. It will show how the DW1000 is being compliant with the IEEE 802.15.4-2011 UWB standard. Second, the environments and the process of the measurements will be introduced in detail. The statistics, which will be collected as a part of the results, will be listed and discussed. Third, theoretical predictions on the possible results of the measurements will be given.

Theory [1] predicts that the overall performance, in the aspect of packets reception percentage, would be better in the multipath propagation environment than in the environment, with little multipath propagation. On the other hand, the performance of the different preamble lengths' synchronization abilities, under those two environments, could not be directly predicted. The conclusions must be made after analyzing the measurement results.

The fourth chapter of this thesis will show the results of both parts' measurements. Based on these results, analysis will be made, and the synchronization ability of the different preamble lengths will be discussed in detail. From the results and analysis of the second parts of the measurements, we will find out how differently the system will perform in a multipath propagation environment from an environment with minimal multipath components.

The fifth chapter of this thesis will be the conclusion part of this thesis. It will not only give a summary on what has been done in this thesis, but also point out the future work needed to be done. The final conclusions on the initial research questions will be given, and those conclusions may hopefully aid the future studies on similar topics.

2. Background study

This chapter mainly focuses on the basic concepts of UWB communications. First, conventional modulation schemes are introduced. Then, several channel models are chosen as candidates for further results analysis. The IEEE 802.15.4-2011 UWB [5] PHY is discussed in detail, while the MAC will be discussed together with the DW1000 MAC features in the next chapter.

2.1. UWB basics

Ultra-wideband technology was used for the radar, sensing, military communications, and niche applications in the 20th century. However, a significant change took place in 2002, when FCC issued a ruling that UWB could be used for data communications as well. [1, 34]

The conventional UWB system operates in the frequency range from 3.1 GHz to 7.5 GHz, while the 60 GHz UWB operates in a much higher frequency range [38]. A band of 7.5 GHz, which surpasses most other current commercial systems, is being allocated to the conventional UWB communications. The maximum allowable transmission power is approximately 0.5 mW [1].

UWB systems often operate at short distances, from 1 m to 10 m, and can offer relatively high data rates. Since the effective isotropic radiated power (EIRP) is very low, multiple UWB pulses are required to carry one bit of information. In order to increase the functional range, one can sacrifice the high data rate by using more pulses to carry the same amount of information.

UWB is commonly based upon impulse radio (IR) schemes. The pulses being applied in IR have very short temporal durations (typically in order of ns), which results in an ultra-wideband spectrum [1, 34]. Certain modulation schemes, such as time-hopping (TH) and direct sequence (DS) can make UWB signals noise-like. The noise-like signals make the detection of the UWB signals difficult, and thus enhances security. Another advantage is that noise-like signals can interfere less with other communication systems.

Due to the extremely large frequencies (several GHz), in which the UWB systems operate, the UWB pulses have very short duration. This means that the UWB signals can be reflected by surfaces, which are separated by a few centimeters. Most objects that we encounter everyday can be regarded as individual reflectors. Thus, an UWB radio channel has extremely rich multipath profile. [1, 34]

Since UWB pulses have very short durations, UWB signals can propagate without additional radio frequency (RF) mixing [1]. Thus, a transceiver in an UWB system can be carrier-less, which leads to low complexity and low cost.

2.2. UWB modulation schemes

UWB systems are typically based on impulse radio (IR) scheme, which refers to the generation of a series of very short pulses. The wide spectrum of the pulse must adhere to a spectral mask requirement. Continuous pulse transmission creates strong spectral lines in the signal's spectrum. [1, 34]

The most common IR based UWB modulation schemes are time-hopping with pulse position modulation scheme, and direct sequence scheme [1]. This section will first

discuss the general principles of IR schemes, and then introduce different data modulation methods. TH-PPM and DS will be discussed in detail, since they are essential to our measurements. Finally, the applications of coherent and non-coherent detection methods will be briefly discussed.

2.2.1. Impulse radio scheme general concepts

Time modulated UWB (TM-UWB) is based upon discontinuous transmission of very short pulses. The most common pulse shape is Gaussian pulse, but there are other candidates, such as Laplacian, Rayleigh, and Hermitian pulses. [4]

One transmitted symbol is spread over *N* pulses to achieve processing gain. This processing gain can combat both noise and interference [15, 17]. According to [4], the processing gain (in dB) acquired from this procedure is defined as

$$PG_1 = 10\log_{10}(N)\,. \tag{2.1}$$

In the TH-PPM modulation scheme, a large time frame is equally divided into small sections, known as burst periods. There is only one burst in a single time-hopping frame. The extremely low duty cycle leads to the reduction of interference caused by any continuous interfering source. According to [4], the processing gain (in dB) due to the low duty cycle is given by

$$PG_2 = 10\log_{10}(\tfrac{T_f}{T_p})\,, \tag{2.2}$$

where T_f is the duration of a time hopping frame, and T_p is the width of the pulse. The total processing gain can be represented as the sum of the two processing gains as

$$PG = PG_1 + PG_2\,. \tag{2.3}$$

Due to the discontinuous transmission of signals, TH-PPM UWB is resistant to severe multipath fading. Moreover, it can take advantage of multipath propagation, as in the case where a non-coherent energy detector receiver is being applied. Inter-symbol interference (ISI) is being avoided, if the time interval between two adjacent bursts is greater than the delay spread.

2.2.2. UWB data modulation

There are mainly three types of UWB data modulation schemes: binary pulse amplitude modulation (BPAM), pulse position modulation (PPM), and pulse shape modulation (PSM) [4]. Since a non-coherent detection receiver is not sensitive to pulse shape, the discussion of PSM will be skipped.

BPAM can be represented by using two antipodal pulses. The on-off key (OOK) modulation can be regarded as a special case of BPAM, where nothing is transmitted when the key is off. According to [4], signal of BPAM is given as

$$x(t) = d_j * w_{tr}(t), \tag{2.4}$$

where $w_{tr}(t)$ represents the UWB pulse waveform, *j* represents the bit transmitted ('0' or '1') and

$$d_j = \begin{cases} -1, & (j = 0) \\ 1. & (j = 1) \end{cases} \tag{2.5}$$

For pulse position modulation (PPM), the position of the UWB pulse determines which bit is transmitted. If bit '0' is represented by generating the pulse at the time 0, bit '1' is shifted by an amount of δ from 0. According to [4], the signal can be represented as

$$x(t) = w_{tr}(t - \delta d_j), \tag{2.6}$$

where d_j is assumed to be the following values, which depend on the bit chosen to be transmitted,

$$d_j = \begin{cases} 0, & (j = 0) \\ 1. & (j = 1) \end{cases} \tag{2.7}$$

The value of δ can be chosen by autocorrelation characteristics [4] of the pulse, which can be defined as

$$\rho(t) = \int_{-\infty}^{\infty} w_{tr}(\tau)\, w_{tr}(t - \tau) d\tau\,. \tag{2.8}$$

For PPM with orthogonal signals, the optimum value of δ can be given as

$$\rho(\sigma_{opt}) = \int_{-\infty}^{\infty} w_{tr}(\tau)\, w_{tr}(\sigma_{opt} - \tau) d\tau = 0\,. \tag{2.9}$$

The autocorrelation functions of the Gaussian waveforms have both positive and negative values. The best BER performance is achieved with the minimum autocorrelation [4].

2.2.3. Time-hopping ultra-wideband

TH-PPM is the fundamental concept of UWB communications. According to previous discussion, a large time hopping frame results in a low duty cycle, which creates processing gain. Spreading the pulses in the time domain also can be regarded as a randomization technique, which reduces the strong spectral lines in the pulse's spectrum. This is due to the fact that, when the transmitted signals are more randomly distributed in time, the spectrum of the transmitted signals becomes smoother.

Fig 2.1 [4] shows the basic concept of TH-PPM UWB. It is shown in the figure that there is only one active burst in each time-hopping frame. The duration of the time hopping frame is much larger than the burst duration, which results in a low duty cycle. The pulse position modulation refers to the modulation of burst positions within each time-hopping frame.

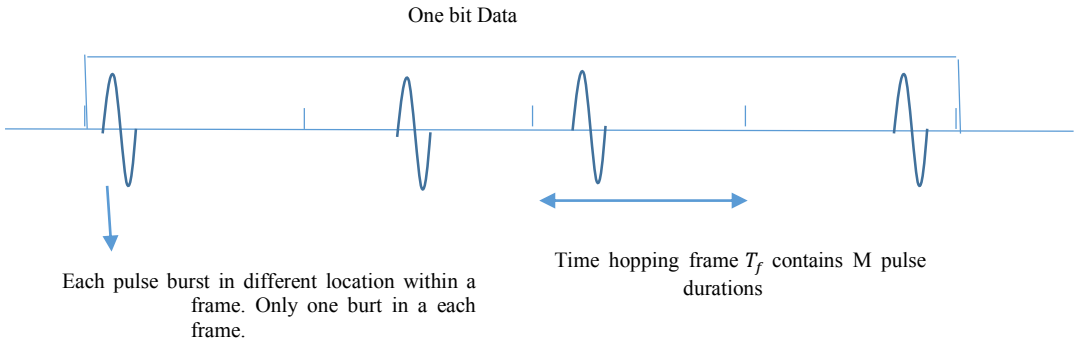

Fig 2.1. TH-PPM concept diagram.

UWB waveforms are generated without additional spreading in frequency domain, which makes the transceiver's structure much simpler [4]. The pulse repetition time is typically much larger than the duration of the pulse. According to [4], the symbol rate of the transmitted signal can be represented as

$$R_s = \frac{1}{T_s} = \frac{1}{N_s T_f}, \tag{2.10}$$

where R_s is the symbol rate, T_s is the symbol duration time, T_f is the duration of the time hopping frame, and N_s is the number of pulses per bit.

According to [4], the information signal *s(t)* for the *m*th user can be described as

$$s^{(m)}(t) = \sum_{k=-\infty}^{\infty} \sum_{j=0}^{N-1} w(t - kT_d - jT_f - (c_w)_j^{(m)} T_c - \sigma {d_k}^{(m)}), \tag{2.11}$$

where T_d is one bit's duration, T_f is the time-hopping frame length, T_c is the chip duration, which is same as the pulse duration, d_k is *k*th data bit, and $(c_w)_j$ is the *j*th chip.

2.2.3.1. Time-hopping UWB multiple access

TH-PPM systems often use pseudo random (PR) codes to separate different users. Within a frame, there are a certain number of transmission instants. So the maximum number of users, which can be allocated into the system without causing interference, equals to the number of transmission instants. [4]

According to [4], the maximum number of non-overlapping users, which is determined by the PR code, is defined as

$$N_U = 2^n - 1, \tag{2.12}$$

where *n* is the number of bits in the PN sequence generator, and N_U is the maximum number of non-overlapping users.

The pulse repetition interval, which defines the length of a single time frame, is the multiplication of the number of users and the length of each time slot (chip). The length of each time slot must be larger than the pulse duration. There also needs to be an additional length of two delay spread periods to avoid ISI. [4]

2.2.4. Direct sequence UWB

A PR code is applied in DS-UWB to spread the consecutively transmitted pulses. The waveform of the pulse takes the role of direct sequence chip. In other words, this technique randomizes the pulses' sequence, without increasing the bandwidth of the system. This is the key feature, which distinguishes the DS-UWB from conventional DS-SS systems.

The spreading of the transmitted signal over a large bandwidth makes the resulting wideband signal appear as a noise signal. In DSSS, the message signal is used to modulate a bit sequence known as the Pseudo Noise (PN) code; this PN code consists of pulses of a much shorter duration than the pulse duration of the message signal. Thus, the pulses of the PN sequence have the effect of chopping up the message signal and resulting in a signal which has a bandwidth nearly as large as that of the PN sequence.

The randomization smoothens the transmitted signal's strong spectral lines, which may interfere with other communication systems at short distances [4, 15]. It also makes the signal more noise-like, which reduces the interference to other communication systems. Fig 2.2 shows the concept of DS-UWB. It is shown in the figure that there are two different cases for direct sequence spreading: the coherent case and the non-coherent case. In the non-coherent case, the spreading of the original data sequence is achieved by adding the scrambling sequence to the original data sequence. In the coherent case, the spreading of the original data sequence is achieved by multiplying the original data sequence by the scrambling sequence. According to [4], the pulse amplitude modulation (PAM) signal s(t) for *m*th user can be presented as

$$s^{(m)}(t) = \sum_{k=-\infty}^{\infty} \sum_{j=0}^{N-1} w(t - kT_d - jT_c)(c_p)_j^{(m)} d_k^{(m)}, \qquad (2.13)$$

where d_k is the *k*th data bit, $(c_p)_j$ is the *j*th chip of the PR code, *w(t)* is the pulse waveform, *N* represents the number of pulses to be used per data bit, T_c is the chip length. The pseudo random code is bipolar assuming values $\{-1, +1\}$, which corresponds to the coherent case in Fig 2.2. The bit length is $T_d = NT_c = NT_p$. In reality, both TH-PPM and DS modulation schemes can be applied together to enhance system performance, as it is in the case of BPM/BPSK [5].

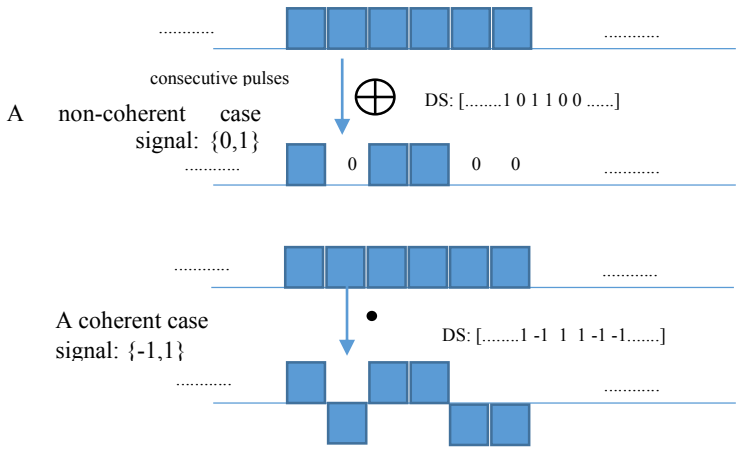

Figure 2.2. DS-UWB concept diagram.

2.2.5. UWB detection methods

UWB detection methods can be summarized as including both coherent and non-coherent schemes, where coherent detecting needs phase recovery, while non-coherent detection does not.

Generally speaking, coherent receiver can offer better performance in terms of the bit error rate (BER) performance and operating range, under noisy channel conditions [19]. It is also resilient to multi-user interference (MUI) [18]. However, it needs a large number of RAKE fingers to detect and recover signals, which leads to high complexity and high implementation cost.

RAKE fingers are sub-receivers, which are correlators each assigned to a different multipath component. Moreover, in order to achieve the mentioned advantages, coherent detection needs perfect estimation of the channel, which is not quite realistic in severe multipath fading environments.

Nevertheless, non-coherent receivers for the UWB can be of low complexity. There are mainly two types of non-coherent receivers for the UWB systems: the autocorrelation receiver (AC) and the energy detection (ED) receiver. AC receivers work by correlating the received signal with its own delayed form, while ED receivers work by squaring the received signal [45]. Both non-coherent detection schemes have poorer BER performance, and are vulnerable to MUI, in comparison with the coherent detection scheme [18]. However, the application of weighted energy detector (WED) can alleviate noise and improve BER performance [45].

Autocorrelation receivers have the advantage of having robustness towards synchronization errors over ED receivers [23]. This is due to the perfect autocorrelation property of the preamble codes [14]. On the other hand, ED receivers can recover all the useful received energy, while AC receivers only get half of that after autocorrelation [20]. This might lead to a lower power consumption of ED receivers over AC receivers.

In conclusion, ED receiver can be regarded as a low complexity and low power consumption option, with a somewhat tradeoff in the detection performance [16]. Such a receiver is being implemented in the DW1000 chipset, which is applied in our measurements.

2.3. UWB channel models

The path loss $PI(f,d)$, which is dependent on frequency and distance, is an important propagation characteristic for the UWB signals. According to Friis transmission formula [23], the path loss can be presented as

$$\frac{P_R(f)}{P_T(f)} = \frac{G_{TX}(f)G_{RX}(f)}{PI(f,d)}, \tag{2.14}$$

where $P_T(f)$ is the transmitted signal power, $P_R(f)$ is the received signal power, and $G_{TX}(f), G_{RX}(f)$ are antenna gains.

This section discusses different UWB channel models from the views of two-ray breakpoint, and multipath propagation. Shadow fading can be another aspect of view, however it does not fit into the indoor environment, where the measurements take place. These models will be useful in further results analysis.

2.3.1. Siwiak Kazimierz UWB two-ray model

In radio communications, the direct line-of-sight ray is not the only ray reaching the receiver, when not in free space. The two-ray ground reflection model, where another ray reflected from the ground reaches the receiver, is a quite useful tool in analyzing the channel. Fig 2.3 [21] depicts the concept of this model. It is shown in the figure that there are two rays reaching the receiver; one is the direct path ray, and the other the ray being reflected by the ground.

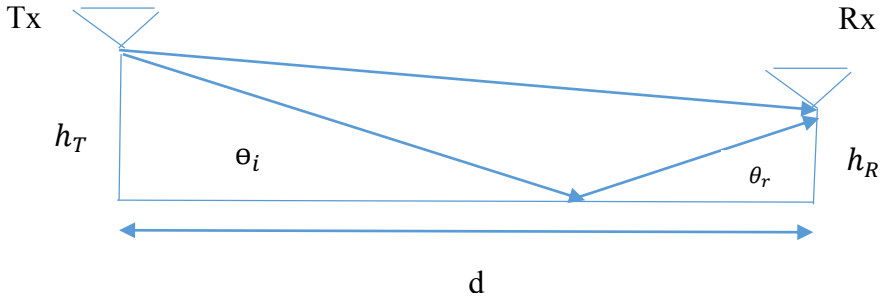

Fig 2.3. Two-ray ground reflection model.

The interference of the reflected path and the direct path depends on their path lengths' difference. According to [21], the normalized amplitude (A) of the received signal is defined as

$$A = 1 + \gamma^2 + 2\gamma\cos({}^{2\pi\Delta L f}/_{c} + \varphi)\,, \tag{2.15}$$

where ΔL is the difference between the reflected path's length and the direct path's length, γ is the magnitude of ground reflection coefficient, φ is the phase of the reflection coefficient. The reflection coefficient is given by [21] as

$$R = \gamma e^{j\varphi}\,. \tag{2.16}$$

Assuming the incident medium is vacuum, and the magnetic permeability, $\mu_1 = \mu_2$ [21]. Then for a horizontally polarized wave, the reflection coefficient is given by

$$R = \frac{\sin(\theta_i) - \sqrt{\varepsilon_r - cos^2(\theta_i)}}{\sin(\theta_i) + \sqrt{\varepsilon_r - cos^2(\theta_i)}}. \tag{2.17}$$

For a vertically polarized wave, R is given by

$$R = \frac{-\varepsilon_r \sin(\theta_i) + \sqrt{\varepsilon_r - cos^2(\theta_i)}}{\varepsilon_r \sin(\theta_i) + \sqrt{\varepsilon_r - cos^2(\theta_i)}}, \tag{2.18}$$

where ε_r is the complex dielectric constant of the reflecting surface. We assume that the wave is horizontally polarized. When d is much larger than the heights of the antennas, θ_i is close to 0, and R is close to -1. This means that the reflected wave is in

opposite phase of the direct path wave. The two waves destruct each other, resulting in the sharp drop of received signal power. At a large distance, the ΔL is approximately

$$\Delta L \approx \frac{2h_t h_r}{d}. \tag{2.19}$$

There needs to be a 180 degree shift in the phase of the reflected wave compared with the direct path wave, in order to cause the maximum reduction in the received signal power. This corresponds to the $(\frac{\lambda}{2} + n\lambda)$'s difference in length between the direct path and the reflected path. When *n* equals 0, the corresponding distance is called the 'first Fresnel zone' distance. This distance is also known as the 'breaking point'. The breaking point can be defined as

$$d_f = \frac{4h_t h_r f}{c}. \tag{2.20}$$

Another way of defining it is

$$d_f = \frac{2\pi h_t h_r f}{c}. \tag{2.21}$$

The above discussion is based upon narrow band signals. However, UWB signals may have a bandwidth over 500Mhz. This leads to the problems of which frequency to choose, and whether the path loss is constant over such a large bandwidth [21].

In the Siwiak Kazimierz (SK) UWB model, the mean value of the narrowband ground reflection model is taken over the bandwidth of UWB. According to [29], this process can be described as

$$PI_{SK} = 10\log\left[\frac{1}{f_H - f_L}\int_{fL}^{fH}\left(\frac{c}{4\pi f d}\right)^2 A(f)df\right]^{-1}, \tag{2.22}$$

where *A* is the same as in (2.15). The mean frequency is defined as

$$f_m = \sqrt{f_H f_L}, \tag{2.23}$$

where f_H and f_L are the high and low frequency -10dB edges. The breakpoint is defined as

$$d_p = \frac{4\pi f_m h_t h_r}{c}. \tag{2.24}$$

2.3.2. Siwiak, Bertoni & Yano UWB model

The SBY model assumes that the amount of rays arriving at the receiver depends on the environment [21]. A full 3-D enclosed environment (e.g. corridor) will act like a waveguide, where all reflections can decrease path loss [30]. According to [30], the path loss of SBY model can be defined as

$$PI_{SBY} = 10\log\left\{\left(\frac{c}{4\pi f_m d}\right)^2\left[1 - exp\left(-\frac{d_p}{d}\right)^{n-2}\right]\right\}^{-1}, \quad (2.25)$$

where d_p is the same as in the SK model, and *n* is the path loss component. When *n*=2, this model agrees with free space model, while *n*=4 means that the environment only contains ground reflection. For the 3-D enclosed environment, *n* is smaller than 2 [24, 27, 30]. It is also concluded, according to [30], that SBY model best describes short range indoor environment**.**

2.3.3. Saleh-Valenzuela model

The S-V model is based on the observation of paths arriving in clusters. According to [21], the channel impulse response (CIR) is given by

$$h(t,\tau) = \sum_{l=0}^{L-1}\sum_{k=0}^{K-1} a_{kl}(t)\delta(t - T_l - \tau_{kl}(t))e^{j\theta_{kl}(t)}, \quad (2.26)$$

where *K* is the number of rays in each cluster, T_l is the arrival time of *l*th cluster, a_{kl} is the amplitude of the *k*th arrival in the *l*th cluster, and θ_{kl} is the phase of the *k*th arrival in the *l*th cluster. The phases are uniformly distributed between [0, 2π], and *L* is the number of clusters of scatters, which is Poisson distributed [21].

The S-V model is adopted by IEEE 802.15.4-2011 UWB specifications in a general form. This general model is designed to work under various conditions, which include indoor residential area, indoor office area, industrial environments, body-area network (BAN), outdoor, and agricultural area. According to [31], the key features of this model are

- Only treating channel, and antenna effects modeled separately.
- d^{-n} law for path loss.
- frequency dependence of path loss.
- Modified S-V model:
    a. arrival of path in clusters.
    b. mixed Poisson distribution for ray arrival times.
    c. possible delay dependence of cluster decay times.
    d. some NLOS environments have first increase, then decrease of power delay profile.
- Nakagami-distribution of small-scale fading, and
- Block fading: channel stays constant over data burst duration.

2.4. IEEE 802.15.4-2011 UWB physical layer

The IEEE standard 802.15.4-2011 [5] UWB physical layer (PHY) waveform inherits the concept of the IR scheme. It currently supports three bands: the sub-gigahertz band (249.6 MHz- 849 MHz), the low band (3.1 GHz- 4.8 GHz), and the high band (6.0 GHz- 10.6 GHz). The sub-gigahertz band supports only one channel, while the low band and the high band support four channels and eleven channels, respectively.

Within each channel, there is support for at least two complex channels, which have unique 31 preamble codes [5]. For a compliant device, it shall at least support one of the channels: channel 0, channel 3, and channel 9. In addition, it shall also support the two unique 31 preamble codes, which are mandatory for the channel. The PHY has another 127 preamble code type, but this is optional.

As introduced earlier in this chapter, TH-PPM and DS are being used together to form the burst position modulation and binary phase-shift keying (BPM/BPSK) modulation scheme, which is applied to support both coherent and non-coherent receivers using a single scheme [5]. In BPM/BPSK, each symbol only consists of one active burst.

2.4.1. UWB physical-layer-convergence-protocol protocol data unit structure

Fig 2.4 [5] depicts the format of the UWB Physical-Layer-Convergence-Protocol (PLCP) Protocol Data Unit (PPDU). It is shown in the figure that both the data field and the physical header are under BPM/BPSK modulation and spreading. However, Reed-Solomon encoding is only applied to data field. All multiple octet fields are transmitted and received with least significant octet first, and each octet is transmitted and received with LSB first. The physical header (PHR) is sent at 850 kb/s for all data rates larger than or equal to 850 kb/s, while it is sent at 110 kb/s for the 110 kb/s data rate.

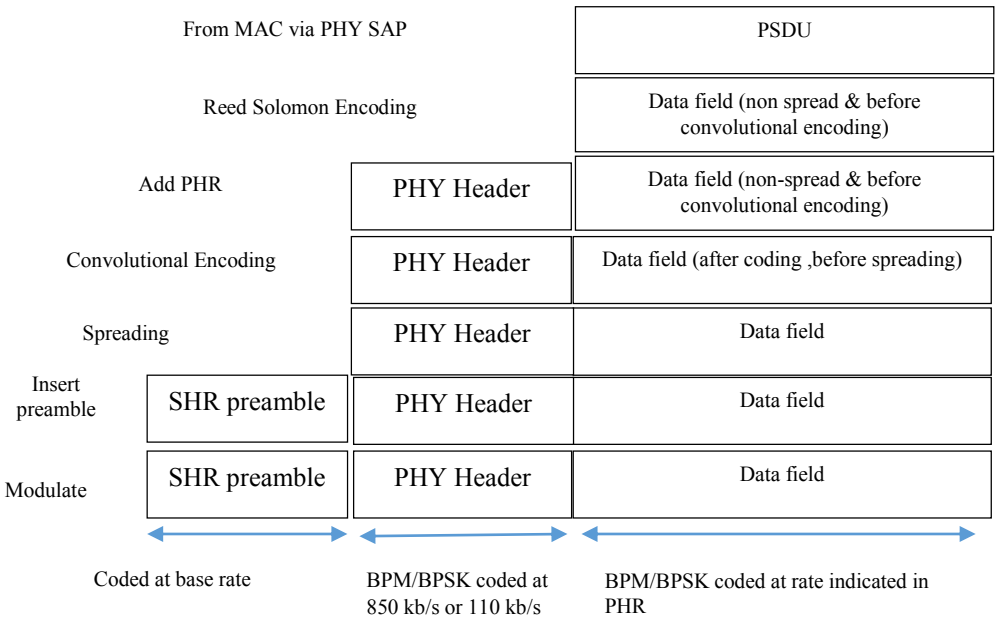

Figure 2.4. Graph of PPDU format.

According to [5], the UWB PPDU encoding process can be summarized as

- Perform Reed-Solomon encoding on PLCP Service Data Unit (PSDU) data units.
- Produce physical header (PHR).

- Add single-error correcting and double-error detecting (SECDED) check bits to PHR and attach the PHR to PSDU.
- Perform convolutional coding.
- Modulate PSDU, and spread it by scrambling PR code. The data rate of PSDU is specified in the PHR.
- Produce preamble field, which is a part of the synchronization (SYNC) field. The SYNC is used for automatic gain control automatic gain control (AGC) convergence, diversity selection, timing acquisition, and coarse frequency acquisition. Start frame delimiter (SFD) is another part of SYNC, and detecting SFD at the receiver is a key event, since it marks the end of preamble demodulation, and the start of data demodulation.

2.4.2. UWB physical layer symbol structure

In the BPM/BPSK modulation, one symbol usually carries two bits of information. In the BPM/BPSK coherent modulation scheme, one bit is used to determine in which time frame a burst will occur, and the other bit is used to modulate the polarity (phase) of that burst. The structure of a UWB PHY symbol is shown in Fig 2.5 [5]. Each symbol has N_c possible chip positions, each with a duration of T_c. Moreover, each symbol is divided into two BPM intervals, each with duration of T_{BPM}.

N_{cpb} consecutive pulses form a burst, which has the duration of $T_{burst} = N_{cpb}T_c$. In the coherent case, a burst can take place in either of the BPMs, resulting in one bit of information. The phase of this burst can be {-1, 1}, which creates another bit of information. Since burst duration is much shorter than BPM duration, ISI and multi-user interference (MUI) can be greatly reduced. This has been discussed in the above section with the case of time hopping. In order to reduce the possibility of interference even more, an additional guard interval, whose duration equals that of the BPM, is attached to the end of each BPM.

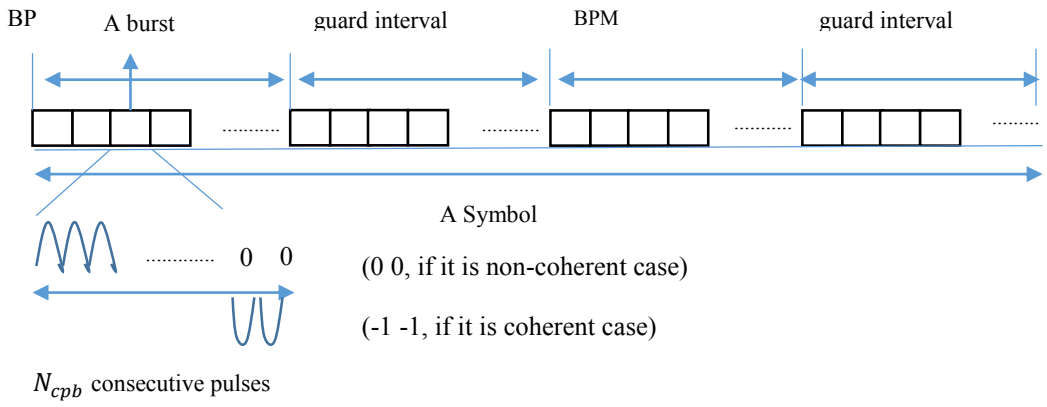

Figure 2.5. UWB symbol structure.

The PSDU's parameters are related to both rate and time. Table 2.1 [5] shows all the necessary PSDU rate-dependent and time-related parameters for our test.

Table 2.1. Time-related and rate-dependent PSDU parameters for test

Channel number	Peak PRF MHz	Bandw-idth MHz	Pream-ble code length	Viterbi rate	RS rate	Overall FEC rate	Burst positi-ons per symbol	Hop bursts	Chips per burst	Chips per symbol	Burst durati-on (ns)	Symb-ol dura-tion (ns)	Symb-ol rate MHz	Bit rate Mb/s	Mean PRF MHz
3	499.2	499.2	31	0.5	0.87	0.44	32	8	16	512	32.05	1025.64	0.98	0.85	15.60

The peak pulse repetition frequency (PRF), which is the inverse of pulse duration, is always 499.2 MHz. The bandwidth denotes the 3 dB bandwidth of the UWB pulses [5]. The mean PRF is defined as the total number of pulses within a symbol divided by the symbol duration. It is important to mention that during the preamble part, the peak PRF and the mean PRF are basically the same, due to the fact that preamble codes are evenly distributed. However, in the data part of a PPDU, the peak and the mean PRFs are different. This is because pulses are grouped into consecutive chip durations.

According to previous introduction, there are two options for the preamble code length, which are 31 and 127. A device, which is compliant with IEEE 802.15.4-2011 UWB standard, must support for the 31 preamble code, with the mean PRFs of 15.6 MHz and 3.90 MHz. The use of 127 code length is optional, and when used, the mean PRF is 62.4 MHz. [5]

Viterbi rate indicates the rate of convolutional encoding. Note that Viterbi rate being equal to 0.5 does not necessarily mean that one symbol can carry two bits of information. In the case of non-coherent modulation, convolution encoding can be done by encoding the even outputs of RS as systematic bits, and odd outputs as polarity bits. In this case, the Viterbi rate is still 0.5, but one symbol can only carry one bit of information. According to [5], the data rate is given by

$$Bit\ rate = 2 * (overall\ FEC\ Rate) * Symbol\ Rate\ . \qquad (2.27)$$

2.4.3. UWB preamble symbol and start frame delimiter structure

A preamble symbol is formed by spreading one whole repetition of preamble codes by delta function σ_L of length L. Table 2.2 [5] shows the preamble parameters.

Table 2.2. Preamble parameters

Channel number	$\mathbf{C}_i$ code length	Peak PRF (MHz)	Mean PRF (MHz)	Delta σ_L length	Chips per symbol	Symbol duration (ns)	Base rate Msymbols/s
{0:15}	31	31.20	16.10	16	496	993.59	1.01
Except 4,7,9,11	31	7.80	4.03	64	1984	3974.36	0.25
{0:15}	127	124.80	62.89	4	508	1017.63	0.98

The preamble code is ternary: {-1, 0, 1}. Table 2.3 [5] shows the code sequence of different code indexes, and the channels where a specific code sequence is assigned.

For each code sequence, there are always 16 active {-1, 1}s, and 15 zeros. The preamble code has a perfect auto correlation property.

Table 2.3. 31 Ternary codes

Code index	Code Sequence	Channel number
1	-0000+0-0+++0+-000+-+++00-+0-00	0,1,8,12
2	0+0+-0+0+000-++0-+---00+00++000	0,1,8,12
3	-+0++000-+-++00++0+00-0000-0+0-	2,5,9,13
4	0000+-00-00-++++0+-+000+0-0++0-	2,5,9,13
5	-0+-00+++-+000-+0+++0-0+0000-00	3,6,10,14
6	++00+00---+-0++-000+0+0-+0+0000	3,6,10,14
7	+0000+-0+0+00+000+0++---0-+00-+	4,7,11,15
8	0+00-0-0++0000--+00-+0++-++0+00	4,7,11,15

The preamble symbol $\mathbf{S}_\mathrm{i}$ is the code $\mathbf{C}_\mathrm{i}$ spread by the delta function σ_L of length L. According to [5], this process is described as

$$\mathbf{S}_\mathrm{i} = \mathbf{C}_\mathrm{i} \otimes \sigma_L(n)\,, \tag{2.28}$$

$$\sigma_L(n) = \begin{cases} 1, & (n = 0) \\ 0. & (n = 1,2,\dots,L-1) \end{cases} \tag{2.29}$$

where $\otimes$ is the Kronecker product.

According to table 2.2 [5], the preamble is transmitted at a slightly higher mean PRF than the data. This is because preamble codes are ternary, not binary. In this case, the mean PRF of preamble can be defined as

$$Preamble\ mean\ PRF = \frac{N_{\{-1,1\}}}{N_C T_C}, \tag{2.30}$$

where $N_{\{-1,1\}}$ stands for the number of {-1, 1}s in a certain code C_i, T_C stands for the duration of a chip, and N_C is the total number of chips within a preamble symbol.

According to previous introduction, detection of SFD is a key event in the receiving process. The SFD is formed by spreading a sequence by $\mathbf{S}_\mathrm{i}$. There are two types of such sequences: the short sequence [0 +1 0 -1 +1 0 0 -1], where the leftmost bit shall be transmitted first in time, is used for transmitting data at default and medium data rates. The long sequence is used for 110 kb/s data rate transmission [5].

2.4.4. Physical header

A PHY header is added after SFD. It consists of 19 bits, and carries information, which is necessary for packet decoding. This information describes the data rate, and duration of the current frame's preamble, and the length of the payload [5]. Since PHR carries crucial information, an addition of six parity check bits (SECDED) are used to protect the PHR against channel errors. The SECDED can correct one error, and detect two errors. Preamble duration indicates the length of the SYNC part in the SHR**.** Fig 2.6 [5] shows the structure of PHR.

Bit 0	1	2	3	4	5	6	7	8	9	10	11	12	13	14	15	16	17	18
R1	R1	L6	L5	L4	L3	L2	L1	L0	RNG	EXT	P1	P0	C5	C4	C3	C2	C1	C0
Data Rate		Frame Length							Ranging Packet	Header Extension	Preamble Duration		SECDED Check Bits					

Figure 2.6. PHR structure.

2.4.5. UWB physical layer modulation

According to [5], in the coherently modulated UWB PHY, the transmitting signal's waveform during the *k*th symbol interval may be expressed as

$$x^{(k)}(t) = \left[1 - 2g_1^{(k)}\right] \sum_{n=1}^{N_{cpb}} \left[1 - 2s_{n+kN_{cpb}}\right] \times p\left(t - g_0^{(k)} T_{BPM} - h^{(k)} T_{burst} - nT_C\right). \tag{2.31}$$

Eq. (2.31) describes the time hopping and polarity scrambling process. According to previous discussion, the processing gain from a low duty cycle and spreading are achieved during this process, thus improving the overall performance of UWB systems.

The *k*th symbol interval carries two information bits: $g_0^{(k)}$ and $g_1^{(k)} \in \{0, 1\}$. Bit $g_0^{(k)}$ is encoded into the burst position, whereas bit $g_1^{(k)}$ is encoded into the burst polarity. The sequence $s_{n+kN_{cpb}} \in \{0, 1\}, n = 0, 1, \ldots, N_{cpb} - 1$ is the scrambling code used during the *k*th symbol interval, $h^{(k)} \in \{0, 1, \ldots, N_{hop} - 1\}$ is the *k*th burst hopping position, and $p(t)$ is the transmitted pulse shape at the antenna input.

The burst hopping sequence $h^{(k)}$ provides for multi-user interference rejection, while the chip scrambling sequence $s_{n+kN_{cpb}}$ not only provides an additional interference suppression, when a coherent receiver is applied, but also smoothens the strong spectral lines of the transmitted signal's spectrum [5].

Fig 2.7 [5] depicts a BPM/BPSK non-coherent modulator. This is based on the fact that non-coherent modulator uses the XOR gate for spreading. It is shown in the figure

that polarity bits and position bits are generated from the FEC encoder. They are being added up by the scrambling sequence through the XOR gate. The CTRL logic determines whether the polarity bit or the position bit modulated.

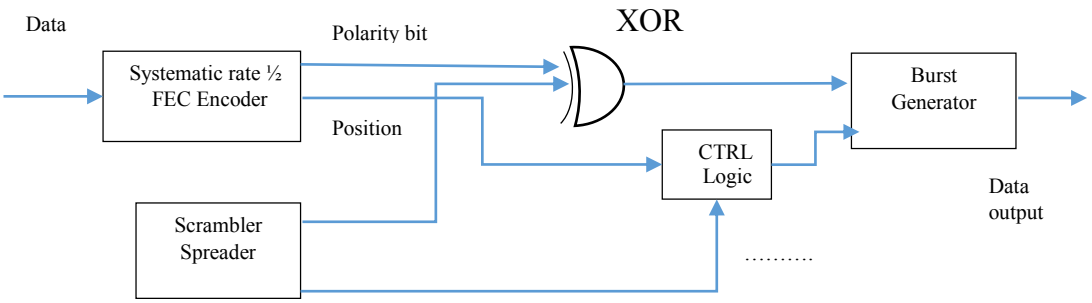

Figure 2.7. BPM/BPSK non-coherent modulator structure.

The spreading sequence and the burst hopping sequence are generated from a common pseudo-random binary sequence (PRBS) scrambler. The polynomial is given by

$$g(D) = 1 + D^{14} + D^{15}\,, \tag{2.32}$$

where D is a single chip delay, T_C, element. This polynomial is primitive, and also forms a maximum length sequence [5]. According to [5], by giving this polynomial, the corresponding scrambler output is generated as

$$s_n = s_{n-14} \oplus s_{n-15}\,. \tag{2.33}$$

The realization of the scrambler is based on a linear feedback shift register (LFSR), which is shown in Fig 2.8 [5]. Upon the transmission of bit 0 of the PHR, the LFSR is initialized, and it will not be reset after the transmission of the PHR [5].

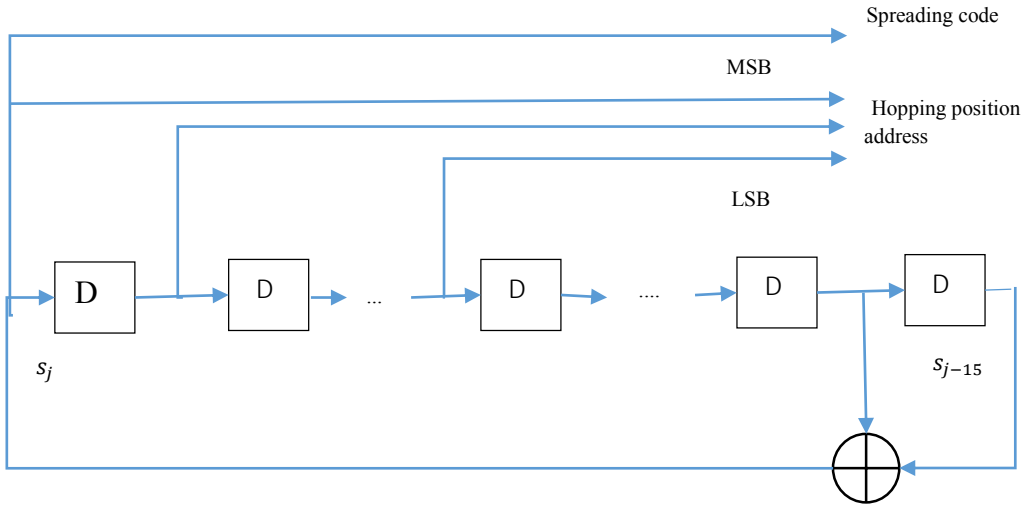

Figure 2.8. Scrambler realized by LFSR.

The initiation seed of the LFSR shall be determined by the preamble code. It is done by removing all the zeros in the ternary code, and then replacing all the negative ones with zeros.

The first 15 bits of the resulting binary sequence shall be loaded into LFSR to create the first state of the scrambler. Even if each device within a PAN uses the same initial LFSR setting, interference is still being rejected by the asynchronous communication within the WPAN [5].

LFSR is clocked at the peak PRF of 499.2 MHz. Within the *k*th symbol interval, the LFSR shall be clocked N_{cpb} times, and the corresponding scrambler output shall be the *k*th scrambling code. According to [5], the *k*th burst hopping position is given by

$$h^{(k)} = 2^0 s_{kN_{cpb}} + 2^1 s_{1+kN_{cpb}} + \cdots + 2^{m-1} s_{m-1+kN_{cpb}}\,, \qquad (2.34)$$

where $m = log_2(N_{hop})$. It is important to point out that for $N_{cpb} < m$, the LFSR is clocked N_{cpb} times, not m times. Correspondingly, the hopping sequences for the mandatory modes with the mean PRFs of 15.60 MHz and 3.90 MHz are given as

$$h^{(k)} = s_{kN_{cpb}} + 2s_{1+kN_{cpb}} + 4s_{2+kN_{cpb}} \;\; (Mean\ PRF = 15.6\ Mhz)\,, \qquad (2.35)$$

$$h^{(k)} = s_{kN_{cpb}} + 2s_{1+kN_{cpb}} + 4s_{2+kN_{cpb}} + 8s_{3+kN_{cpb}} + 16s_{4+kN_{cpb}} \quad (Mean\ PRF = 3.9\ Mhz). \qquad (2.36)$$

2.4.6. UWB physical layer forward error control

The inner convolutional encoder shall use the rate 0.5 code with polynomials: $g_0 = [\,0\ 1\ 0\,]_2$ and $g_1 = [\,1\ 0\ 1\,]_2$. The encoder shall be initialized to the all zero state, upon transmission of each PPDU. This is done by appending two zero bits to the PPDU. [5]

Fig 2.9 [5] depicts the process, where a block of M PSDU (or MPDU) bits, $b_0, b_1, \ldots, b_{M-1}$ go through FEC encoding. The Reed-Solomon encoder shall append 48 parity bits to the block. It is mentioned earlier that in the case of non-coherent modulation, even outputs of the RS encoder are used for encoding the burst positions, while odd outputs shall be used to encode the polarity bits. *M* shall always be an even number [5].

Based on previous discussion, in the non-coherently modulated UWB PHY, the transmitting signal's waveform during the *k*th symbol interval may be expressed as

$$x^{(k)}(t) = \begin{cases} \sum_{n=1}^{N_{cpb}} s_{n+kN_{cpb}} \oplus p\left(t - g_0^{(k)} T_{BPM} - h^{(k)} T_{burst} - nT_C\right), & if\ k\ is\ even \\ \sum_{n=1}^{N_{cpb}} s_{n+kN_{cpb}} \oplus p\left(t - g_1^{(k)} T_{BPM} - h^{(k)} T_{burst} - nT_C\right), & if\ k\ is\ odd \end{cases} \qquad (2.37)$$

where definitions of Eq. (2.31) also apply.

The systematic Reed-Solomon code is over the Galois field, GF(2^6). According to [5], the polynomial of the systematic RS code is given as

$$g(x) = \prod_{k=1}^{8}(x + \partial^k) = x^8 + 55x^7 + 61x^6 + 37x^5 + 48x^4 + 47x^3 + 20x^2 + 6x + 22\,, \quad (2.38)$$

where ∂=010000 is a root of the binary primitive polynomial 1+x+x^6 in GF(2^6) [5].

In RS encoding $RS_6(K+8, K)$, (330-I) redundancy bits are added to each I bits of information, forming a 330 bits' RS block. Each RS block is then converted into K symbols, with $K=\lceil I/6 \rceil$. Here, K equals 55. After RS encoding, there are 48 bits being appended to the original I bits' block [5]. Each K symbols' RS block can correct up to 4 (8/2) symbol errors, and detect 8 symbol errors. If the number of symbol errors exceeds the RS block's error correction capability, the RS block fails. The RS encoding has the characteristic of being robust to consecutive burst errors. This is due to the fact that a symbol can have all its bits wrong, and that still counts as one symbol error.

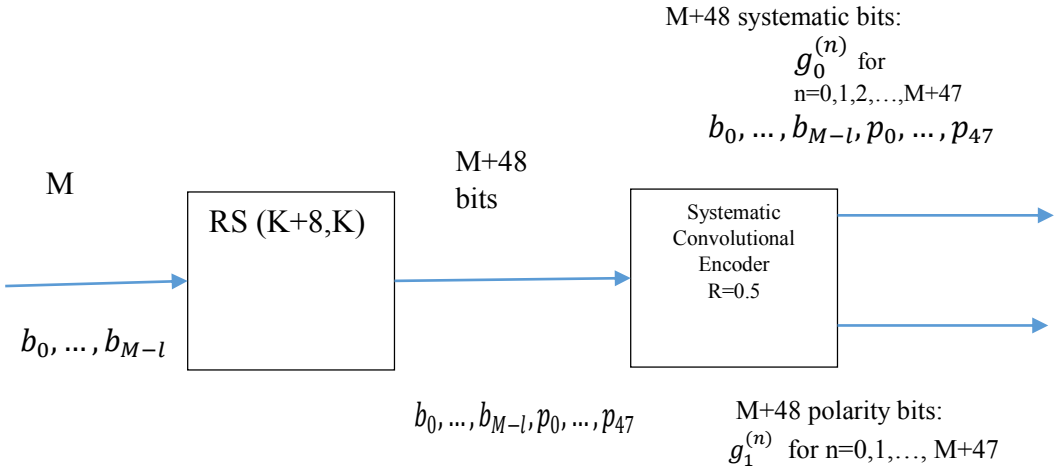

Fig 2.9. Diagram of the FEC encoding process.

3. Measurement settings

First, this chapter gives an overall introduction of the DW1000 chipset, which includes its hardware, as well as MAC features. Second, based on the purposes of the measurements, two different scenarios and key parameters of the measurements are shown. The purposes of the measurements are to study the synchronization ability of different preamble lengths in an environment with minimal multipath components, and to study the performance of the system in an environment with rich multipath components. Finally, theoretical predictions on results are made, which are based upon analysis of the second chapter's channel models.

3.1. DW1000 chipset

Being Compliant with the IEEE802.15.4-2011[5] UWB standard, DW1000 is a low-power, fully integrated, single chip CMOS radio frequency (RF) transceiver integrated circuit (IC) [7]. Fig 3.1 shows the image of the whole device, which includes the DW1000 and its antenna. Fig 3.2 [7] shows the brief structure of the device.

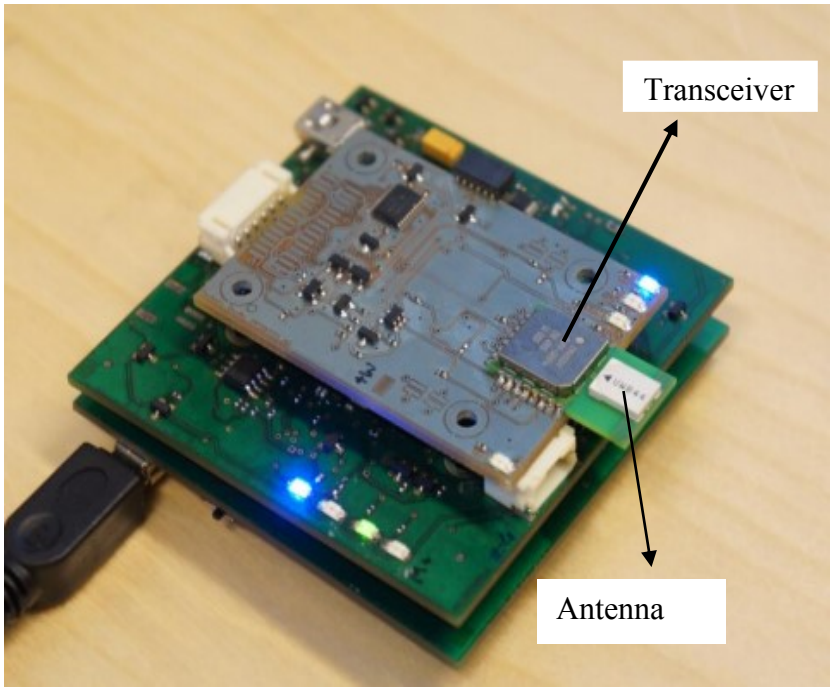

Figure 3.1. Image of the DW1000.

DW1000 mainly consists of two parts: the transceiver, and the host interface. The transceiver is made up of a transmitter and a receiver. A switch is applied to connect the transmitter or receiver to the antenna port [7].

The RF front end of the receiver amplifies the received signal in a low-noise amplifier, before down-converting it directly to baseband [7]. This stage involves automatic gain control (AGC). The AGC needs a certain period of time, known as the settling time, to converge [2]. If the settling time is too short, the amplification of

received signal might not be sufficient. The receiver is optimized for wide band, linearity, and noise figure, allowing IEEE 802.15.4-2011 UWB channels to be down-converted with minimum addition of noise and distortion [7].

The host interface is connected to an off-chip processor (i.e. laptop). The host processor gets the received data from the slave-only Serial Peripheral Interface (SPI). This SPI is used for configurations. The functions of the MAC include CRC generation, CRC checking, and frame filtering. [7]

The DW1000 contains a local oscillator (LO), which is generated by the synthesizer (RF PLL/Synth). This (LO) provides specific center frequencies for the channels under IEEE802.15.4-2011 [3] UWB. The CLK PLL/Synth, however, is used for signal processing. During the SLEEP state, the device uses an external 13 KHz oscillator [7].

One-time programmable (OTP) chip exists on the device. It is used to store calibration data such as TX power level, range accuracy adjustment information, and crystal initial frequency error adjustment. The Always-On (AON) memory is configurable, and it can be used to store DW1000 configuration data during the lowest power operational states. [7]

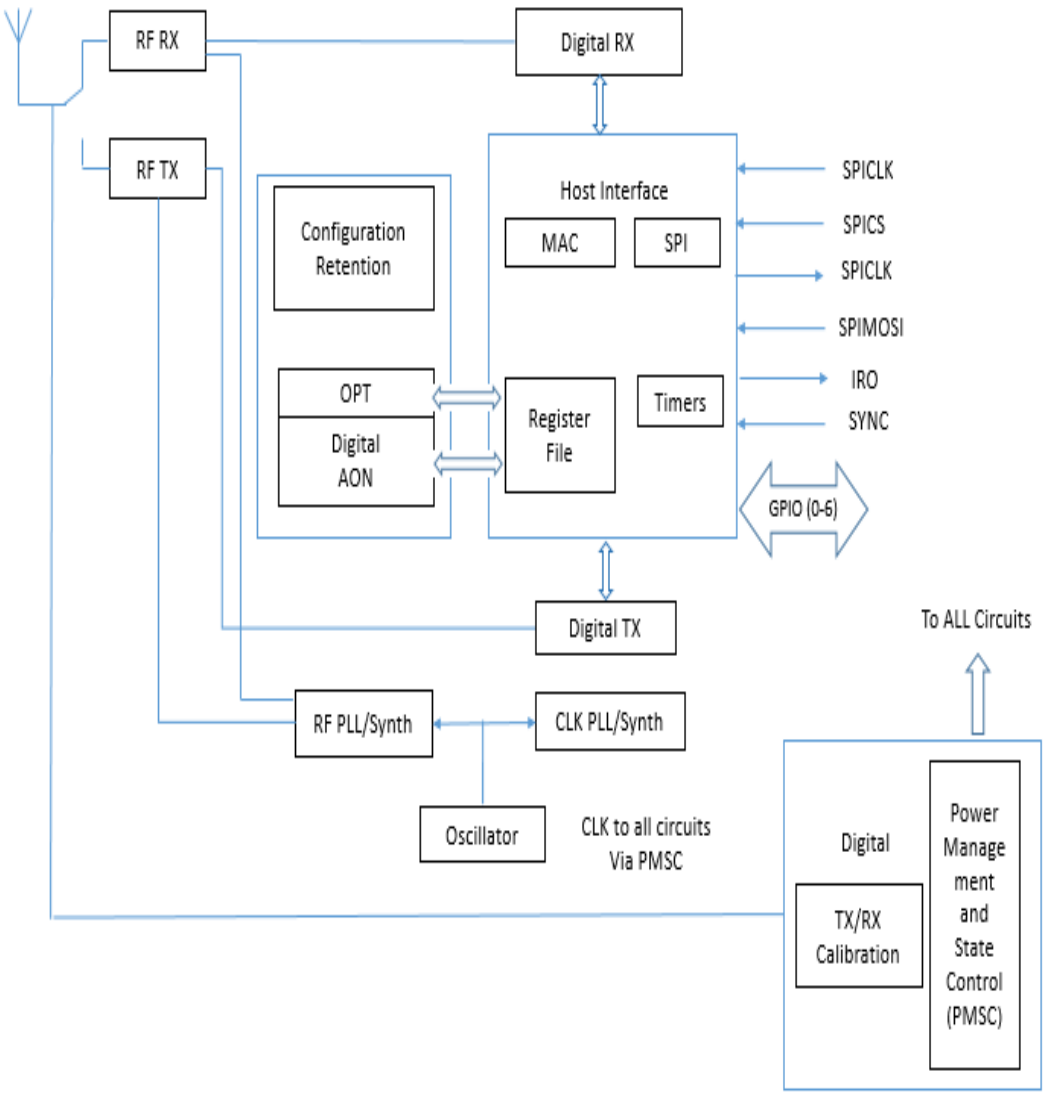

Figure 3.2. Brief structure of the DW1000.

3.2. DW1000 operating states

Fig 3.3 [8] shows the DW1000's operational states (from OFF to IDLE), and Fig 3.4 [8] shows the DW1000's operational states from IDLE to SLEEP or DEEPSLEEP. According to [8], the operational states are described as

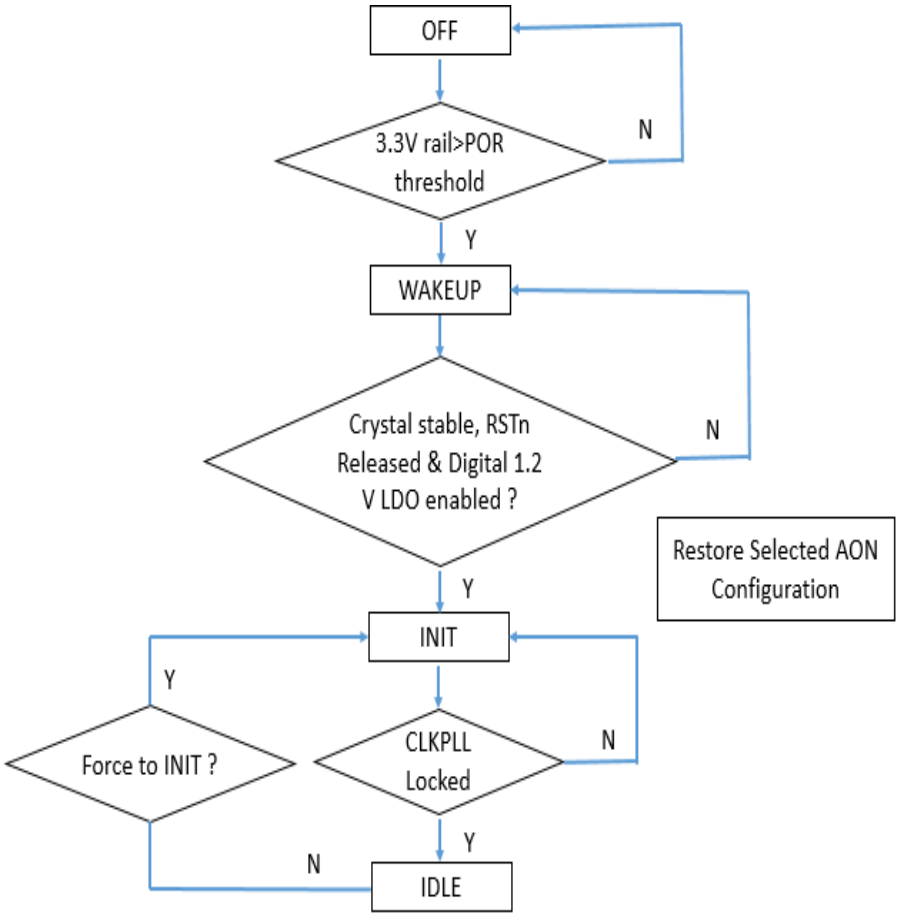

Figure 3.3. Diagram of operational states from OFF to IDLE.

1. WAKEUP: This state is a preparation stage for INIT.
2. INIT: The preparation to enter IDLE. SPI access is available, but the SPI's clock (SPICLK) input frequency is limited to no greater than 3MHz.
3. IDLE: In this state, the clock phase-locked loop (CLKPLL) is locked running and ready for use [8]. However, the CLKPLL is gated off to most circuitry, in order to save energy [8]. The SPI transactions will operate at largest SPICLK frequency, which is 20 MHz. As for the analog transmit and receive circuits, they are powered down in this state.
4. Difference between SLEEP and DEEPSLEEP: In SLEEP state, an internal oscillator is running, which acts as the sleep counter clock. When it expires, the DW1000 will wake up. However, in DEEPSLEEP, all internal circuits are turned off, except for the always-on (AON) circuit, which configures the wakeup restoration [8].
5. TX: In this state, the DW1000 will transmit a frame.

6. RX: In this state, the DW1000 will search for preamble and SFD. After receiving and decoding the PHR, it will receive the data payload. After reception ends (either receiving a good frame, or some error or timeout event that will abort the reception), the DW1000 will return to IDLE state. [8].
7. SNOOZE: A counter is set at the end of reception complete, and after its expiration, the device will return to RX state again through INIT and IDLE.

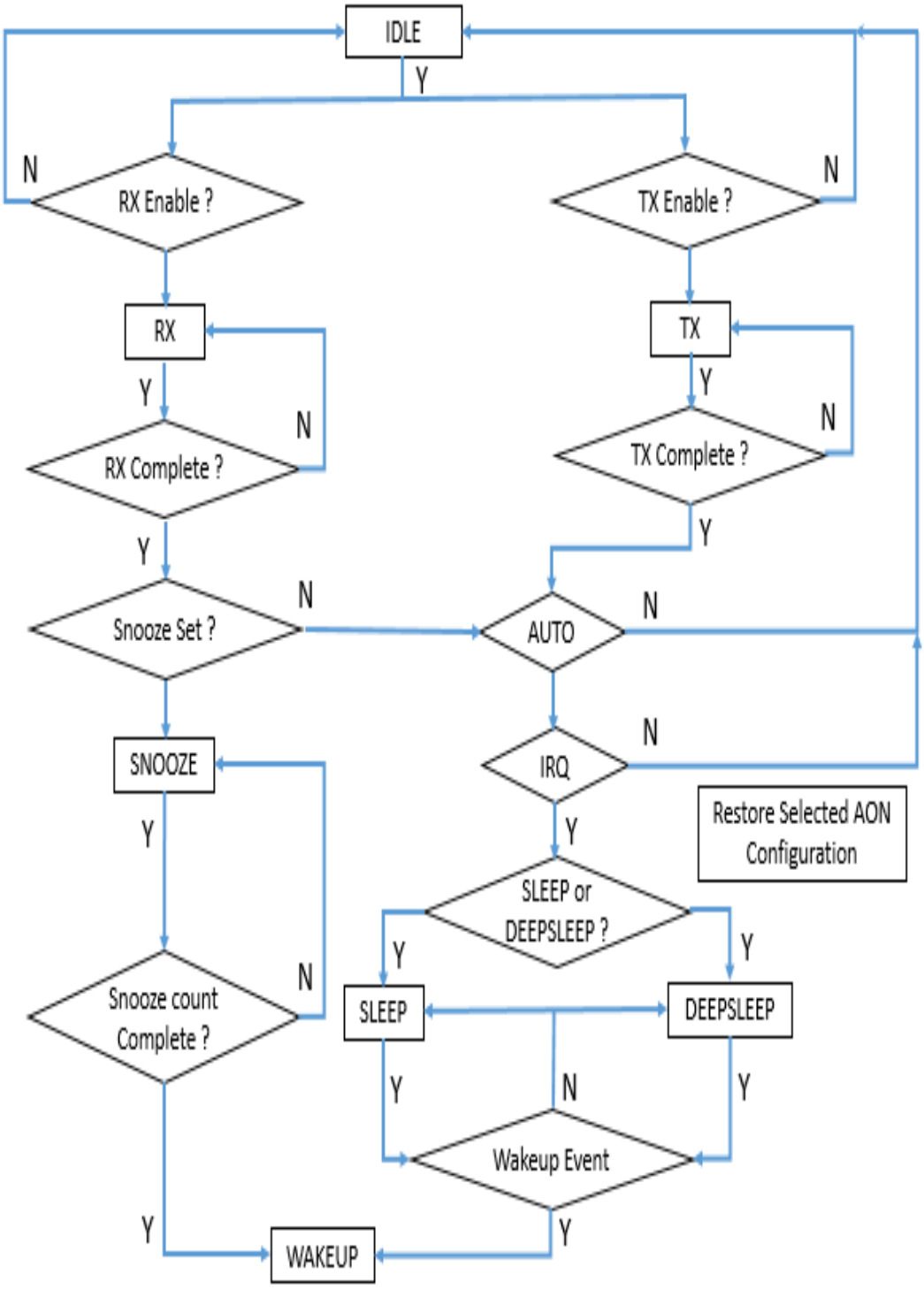

Figure 3.4. Diagram of IDLE, reception, and transmission process.

3.3. Message reception

The reception of a frame is enabled either by an automatic re-enabling of the receiver, or by a host request [10]. Fig 3.5 [10] shows the flow chart of the reception steps.

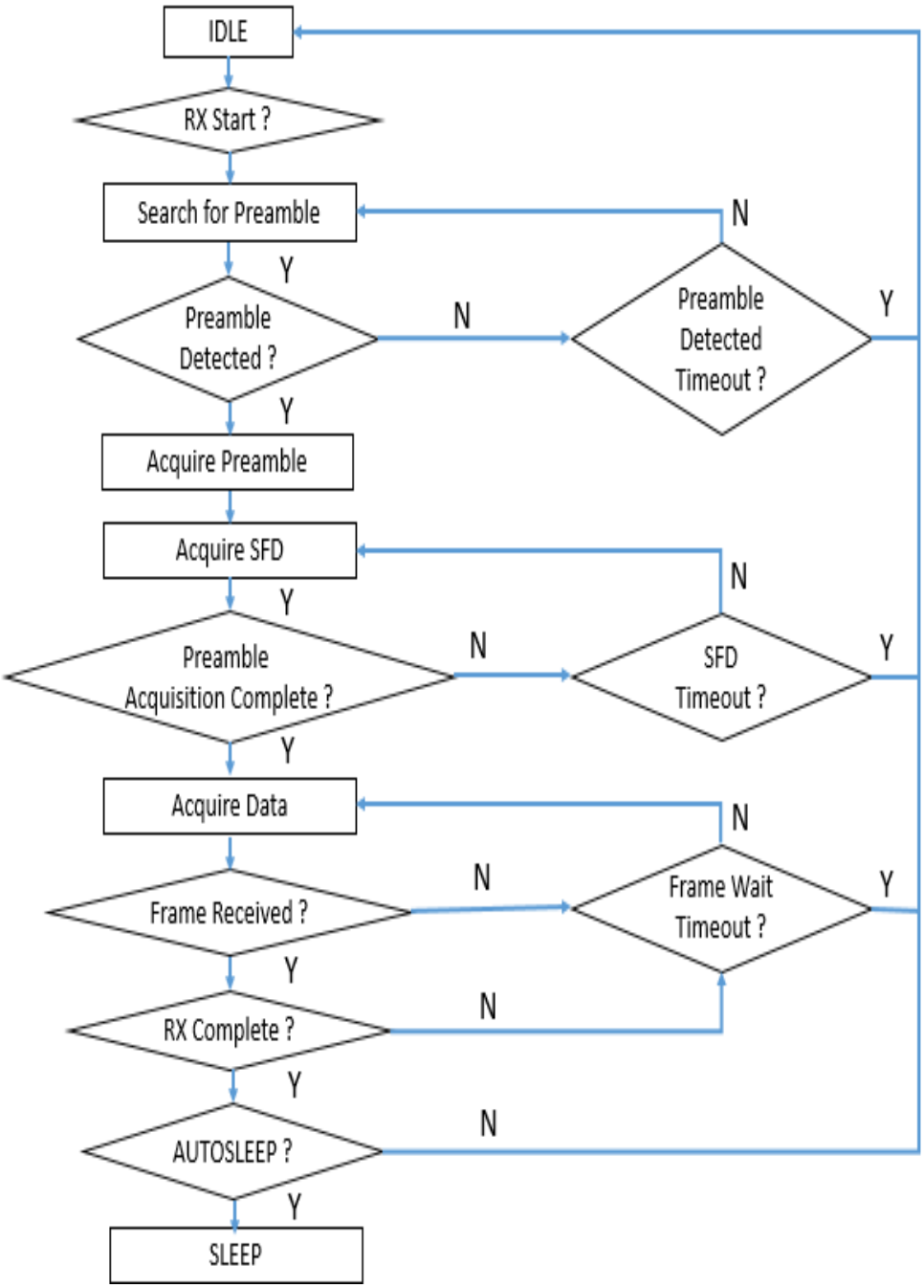

Figure 3.5. Diagram of message reception process.

The device will search for preamble continuously until one has been detected. However, if a preamble detection timeout is set, the receiver will stop searching for a preamble when the search duration has exceeded the timeout.

A preamble is detected by cross-correlation, where preamble is cross-correlated with chunks that are a number of preamble symbols long. The length of the chunk is determined by the preamble accumulation chunks (PAC). A larger PAC size may offer better performance. However, if a PAC is too large for a certain preamble length, the performance of the receiver would be impaired. Table 3.1 shows the recommended PAC sizes for the preamble lengths. [10]

Table 3.1. Recommended PAC size

Expected Preamble length	PAC size
64	8
128	8
256	16
512	16
1024	32
1536	64
2048	64

Once a preamble is detected, the receiver begins accumulating preamble symbols, meanwhile looking for the SFD sequence. Accumulation is halted when the SFD has been detected, but may halt earlier if the accumulated energy in the accumulator grows too fast, as is in the case of close LOS conditions. In this case, the receiver continues receiving preamble symbols, without accumulating them. [10]

Like the setting of preamble detection timeout, there is also the SFD detection timeout. If the SFD is not detected within a certain period of time after the preamble is detected, the reception is aborted. The use of SFD timeout is to prevent false detection of the preamble. [10]

When the auto-acknowledgement function is enabled, a source node will wait for the ACK from the destination node after sending each packet. If the source node has not received ACK from the destination node within a certain period of time (frame wait time), the transmitter will send the same packet again.

3.3.1. RX timestamp

During a transmission, a time-stamp is used to mark the start of the PHR. It is defined as RMARKER. Thus, during the reception, the detection of SFD becomes very important. Because it marks the start of PHR, which is RMARKER [10]. The ability to receive the time stamping is one of the DW1000's external synchronization functions [12].

The IEEE 802.15.4 UWB standard nominates the time when the RMARKER arrives at the receiver as the important event that is time-stamped. Based upon this timestamp, the DW1000 can make corrections, such as subtracting the receive antenna delay and adding the correction factor given by the first path detection algorithm [10] embedded within the device.

A more accurate RX timestamp allocation, not only aids synchronization, but also provides a better first path resolution. According to [10], the estimation of the first path signal power (in dBm) is given as

$$First\ Path\ Power\ level = 10 * log_{10}\left(\frac{F_1^2+F_2^2+F_3^2}{N^2}\right) - A\,, \tag{3.1}$$

where N is the value of 'Preamble Accumulated' counter during each packet transmission. A is constant 115.72 for the 16 MHz PRF, and 121.74 for the 64 MHz PRF.

F1 (*F2* and *F3*) is the First Path Amplitude point 1 (point 2 and point 3) magnitude value reported in the FP_AMPL1 (FP_AMPL2 and FP_AMPL3) field of the register file [13]. According to [10], the estimation of received signal power (in dBm) is given as

$$RXLevel = 10 * log_{10}\left(\frac{C*2^{17}}{N^2}\right) - A\,, \tag{3.2}$$

where C is the channel impulse response value.

It is possible to identify whether a channel is line-of-sight (LOS) or non-line-of-sight (NLOS), based on comparing first path power level with received power level. According to [10], the identification of a LOS or NLOS channel is given by

$$\begin{cases} (RXLevel - First\ Path\ Power\ Level)_{LOS} < 6, \\ (RXLevel - First\ Path\ Power\ Level)_{NLOS} > 10. \end{cases} \tag{3.3}$$

3.3.2. Double buffer

There are a pair of receive buffers in the DW1000. The double receive buffers can enable the device to read previously received data, while using the other one to receive currently transmitted data [10]. The purpose of applying the double receive buffers is to avoid any blink message [10]. Suppose in a single receive buffer's case, where the transmitter is sending messages constantly, the single receive buffer will not be able to receive a message, if it is currently reading the previous data.

The DW1000 often operates in a single buffer mode by default, and it fits many applications [10]. When using the double buffer mode, it is appropriate to configure the DW1000 to automatically re-enable the receiver once it has completed receiving any previous frame [10].

There is also a buffer pointer index indicating which buffer the receiver is using, and controlling which buffer to use for the next frame. This is the ICRBP bit [10]. Successful reception of a new frame with good CRC will cause the ICRBP bit to increase, while the reception of a rejected frame (either caused by bad CRC or frame filtering) will not change the ICRBP bit, and the receiver will use the same buffer for the next frame [10].

3.3.2.1. Overrun

An overrun is the situation where the receiver cannot keep up with the arrival rate of frames. For instance, the receiver receives a frame in the first buffer, moves on to the other buffer and places a received frame in it, too. The receiver will move back to the first buffer again. If the host has not completed reading the data from this buffer, the receiver will not overwrite that buffer with any new frame. If a new frame arrives at

this point, the receiver is unable to write data to the buffer, which leads to an overrun situation [10].

If an overrun occurs, the ongoing frame reception will be aborted [10]. Assuming RX auto-re-enable is enabled, the receiver will look for preamble again. The overrun causes the corruption of good frames previously received, and in this case, the received frames must be abolished [10].

3.4. Media access control hardware features

Fig 3.6 [7] shows the PHY Protocol Data Unit (PPDU). The PPDU is made up of a synchronization header (SHR), a physical header (PHR), and a MAC protocol data unit (MPDU). Reed-Solomon encoding is only applied to the MPDU. The SHR contains the preamble sequence and the SFD.

Fig 3.7 [7] shows the MAC Protocol Data Unit (MPDU) applied for the DW1000 (the Auxiliary Security Header is not processed in DW1000 hardware) [7]. The maximum length of the MPDU is 127 bytes [7]. In our measurement, each test packet includes 11 bytes of overhead: 2 bytes' frame control, 1 byte's sequence number, 2 bytes' destination address, 2 bytes' source address, 2 bytes' PAN ID, and 2 bytes' FCS. Thus the maximum payload is therefore 116 bytes.

Fig 3.8 [6] shows format of the frame control field, which is two octets long. The frame control field contains important information such as frame type and addressing modes. Table 3.2 [6] shows different frame types within the frame control field.

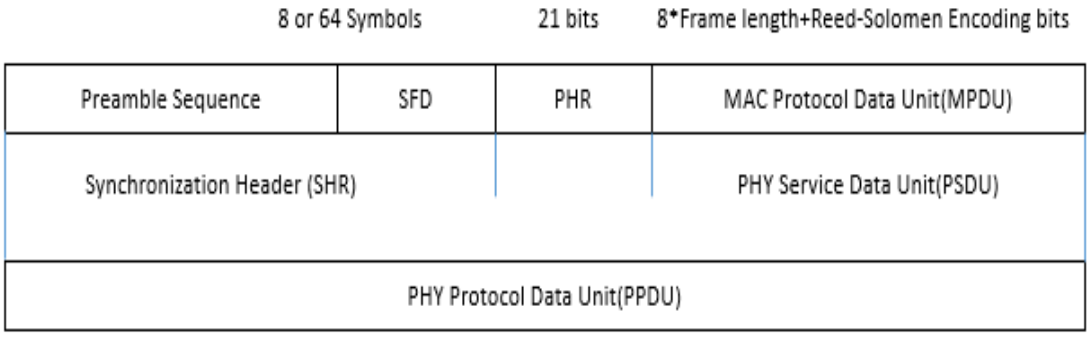

Figure 3.6. Diagram of the PPDU structure.

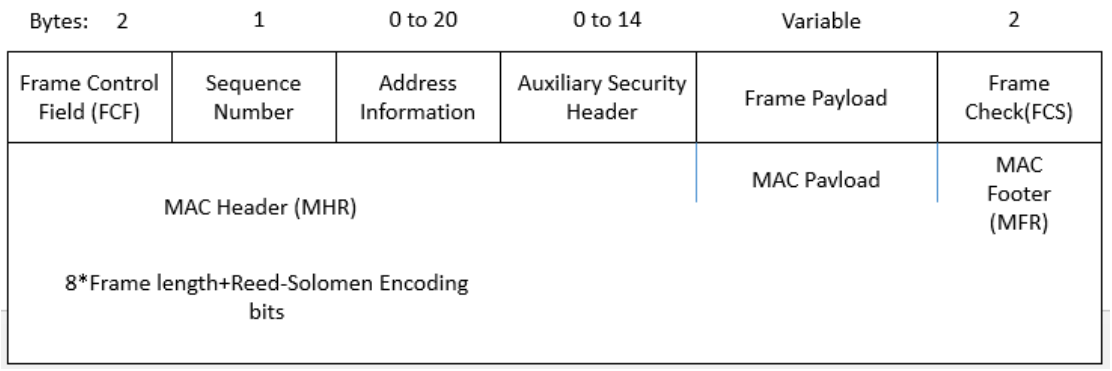

Figure 3.7. Diagram of the MPDU structure.

Bits: 0-2	3	4	5	6	7-9	10-11	12-13	14-15
Frame Type	Security Enabled	Frame Pending	AR	PAN ID Compression	Reserved	Dest. Address Mode	Frame Version	Source Addressing Mode

Figure 3.8. Diagram of Frame Control Field structure.

Table 3.2. Values of the Frame Type Field

Frame type value	Description
000	Beacon
001	Data
010	Acknowledgement
011	MAC command
100-111	Reserved

The DW1000 is capable of automatically calculating and appending the 16 bit CRC frame check sequence (FCS) at the end of each transmitted frame [11]. The destination node compares the calculated CRC with the final two octets of the received frame to check whether they match or not. A match up indicates that a good frame has been received. Otherwise, there are errors in the received frame, and the received frame will be discarded.

The FCS contains a 16-bit ITU-T CRC, and it is calculated over the MHR and MAC payload parts of the frame. According to [5], standard polynomial of degree 16, which is used to calculate FCS, is given by

$$G_{16}(x) = x^{16} + x^{12} + x^5 + 1\,, \tag{3.4}$$

and the algorithm [6], which is used to check the FCS, is described as

- Let $M(x) = b_0x^{k-1} + b_1x^{k-2} + \cdots + b_{k-2}x + b_{k-1}$ be the polynomial representing the sequence of bits for which the checksum is to be computed,
- Multiply $M(x) by\ x^{16}, giving\ the\ polynomial\ x^{16} \times M(x)$,
- Divide $x^{16} \times M(x)$ modulo 2 by the generator polynomial, $G_{16}(x)$, to obtain the remainder polynomial, $R(x) = r_0x^{15} + r_1x^{14} + \cdots + r_{14}x + r_{15}$,
- FCS field is given by the coefficients of the remainder polynomial, $R(x)$.

Fig 3.9 [6] shows the implementation for generating the FCS. The process below shows how the DW1000 is capable of automatically calculating and appending the 16 bit CRC frame check sequence (FCS) at the end each transmitted frame [9, 11]. According to [6], the steps of generating the FCS are

- Initialize the reminder register to zero,
- Shift MHR and payload into the divider in order of transmission (LSB first),
- After the last bit of the data is shifted into the divider, the reminder contains FCS,
- The FCS is appended to the data so that r_0 is transmitted first.

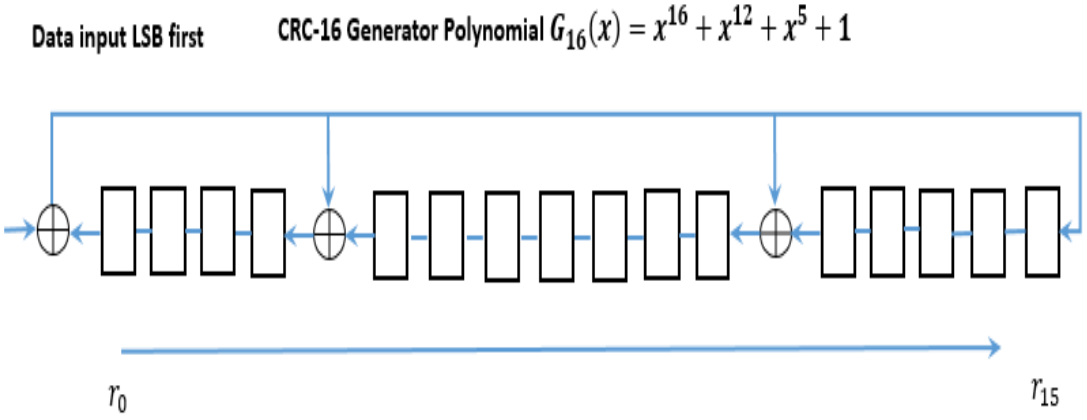

Figure 3.9. Diagram of FCS generation.

Frame filtering is an important feature of DW1000 [11]. The receiver only accepts the frames that pass through frame filtering rules [11], which include

1. The frame type must be allowed for reception:

   - The FFAB [13] bit must be set to allow a Beacon frame to be received.
   - The FFAD [13] bit must be set to allow a Data frame to be received.
   - The FFAA [13] bit must be set to allow an ACK frame to be received.
   - The FFAM [13] bit must be set to allow a MAC command frame to be received.
   - The FFAR [13], FFA4 [13], and FFA5 [13] are set to allow reserved types to be received, excluding those rejected due to frame length check.
   - *NB: In Frame types 0-3, which refer to frame type table, frame header is also used to determine the size of the received frame, and reject the frame if it is shorter than expected.*

2. The frame version field must be correct.
3. The Destination PAN_ID must be either the broadcast PAN_ID, or matching the PAN_ID programmed in the register file [13].
4. The Destination Address must be either the short 16-bit broadcast address, or a short 16-bit address, which matches the SHORT_ADDR programmed in the register file [13]. The Destination Address can also be a long address, which matches the extended unique identifier in the register file [13].
5. If the frame is a beacon frame, the Source PAN_ID must match the programed PAN_ID in the register file [13].
6. If only the source address is present, the receiver will accept the frame as the role of a 'coordinator'. In addition, the Source PAN_ID must match the programed PAN_ID in the register file [13].
7. The FCS (CRC) must be correct in order for the frame to be accepted.

After the frame control field and the address filed in the MHR are received and decoded, the destination node will make decision on whether to accept a frame or not, according to the FFR's addressing rules. When a frame is rejected, the reception

process is aborted immediately. Thus, the frame filtering can prevent a prolonged listening of the destination node. [11]

The automatic acknowledgement function is another important feature of the DW1000 [11]. It will only operate when both frame filtering and automatic acknowledgement functions are enabled. The device will transit into transmit mode after receiving and validating a frame (that includes an acknowledgement request), and send a 5-octet MAC acknowledgement frame [11]. The auto-acknowledgement and double receive buffer can be used together in the situation with overruns taking place. If an overrun occurs, the device will send the acknowledgement of receiving a good frame, and then abort the received frame.

RX auto-re-enable function allows the DW1000 to switch automatically between the receive mode and the transmit mode. In the situation where auto-acknowledgement and frame filtering are both enabled in the double buffer mode, the device will automatically transit from the receive mode into the transmit mode to send the acknowledgement frame after each successful reception. When the transmission finishes, the DW1000 will automatically return into the receive mode again [11].

A frame pending bit is included in the frame control at the start of each frame [6]. This bit can be used in the case of auto-acknowledgement to indicate that the responding node has data to send to the node requesting the ACK. This bit is zero by default, and it is required to be configured when it is needed [11].

3.5. Physical layer hardware features

The DW1000 supports the following six IEEE 802.15.4-2011[5] UWB channels, as shown in Table 3.3 [7]. It also supports IEEE 802.15.4-2011[5] UWB bit rates of 110kbps, 850 kbps and 6.81 Mbps and nominal PRF values of 16 and 64 MHz, as shown in Table 3.4 [7].

In general, low data rates offer increased receiver sensitivity, increased link margin and longer range [7]. However, a lower data rate means that more pulses are combined to carry one bit of information. Thus a lower data rate increases the channel occupancy time.

Based on previous introduction, the preamble sequences are generated by spreading preamble codes. On each channel, two preamble codes are defined for the 16 MHz PRF, and four preamble codes are defined for the 64 MHz PRF [5]. These codes are ‘semi-orthogonal’, which allows devices on the same channel to use different preamble codes to operate simultaneously as if on separate channels [14]. The perfect periodic auto-correlation property of the preamble sequences allows the receiver to accumulate preamble symbols while creating an accurate model of the channel impulse response [14]. This is the key for the DW1000’s good long-range performance, and accurate calculation of the first path arrival time for the RX timestamp allocation.

The preamble length has a huge effect on the operational range and accuracy of RX timestamp allocation. Generally, longer preambles improve range performance, and offer better first path arrival time information. However, longer preamble lengths result in longer channel occupant time and higher power consumption [14]. For 850 kbps data rate, the recommended optimal preamble length is 256 or 512 or 1024 [14].

Both the 16 MHz PRF and the 64 MHz PRF can coexist on the same channel without interference. Compared with the 64 MHz PRF, the 16 MHz PRF reduces the transmitter’s power consumption [7]. However, the 64 MHz PRF gives more accuracy on the first path timestamp allocation [14].

Table 3.3. Supported UWB channels by the DW1000

UWB Channel Number	Center Frequency (MHz)	Bandwidth (MHz)
1	3494.4	499.2
2	3993.6	499.2
3	4492.8	499.2
4	3993.6	1331.2
5	6489.6	499.2
7	6489.6	1081.6

Table 3.4. Supported bit rates and PRF modes by the DW1000

PRF (MHz)	Data Rate (Mbps)
16	0.11
16	0.85
16	6.81
64	0.11
64	0.85
64	6.81

.

3.6. Measurement topology

IEEE 802.15.4-2011 UWB is a special standard that can take advantage of multipath propagation, due to its special PHY layer structure. One of the purposes of the measurements is to find out how multipath propagation would affect the system. Moreover, other possible factors during the test, such as ISI and interference from other systems are taken into account as well.

3.6.1. Test constant parameters

There were two DW1000 devices involved in the measurements, which acted as nodes. One was defined as a SINK node, and the other was defined as an END node. They both transmitted and received frames. The desired preamble lengths to be tested are 64, 256, 512, 1024, 1536, and 2048. The measurements' constant parameters during both two scenarios are

1. Test channel: channel 3, which is the mandatory low-band channel.
2. Center frequency: 4492.8 MHz.
3. Bandwidth: 499.2MHz.
4. Data rate: 850kbps.
5. Burst positions per PHR and MPDU symbol: 32.
6. Chips per burst: 16.
7. Number of possible burst positions per PHR and MPDU symbol: 16.

8. Data payload size: 116 bytes, taking into account the 11 bytes' header, which makes up the maximum length of 127 bytes' frame.
9. ACK: the acknowledgment is enabled.
10. Number of transmitted packets per measurement: 4000. The maximum number of packets that the memory can hold at a time is 8000. 4000 is chosen so the transmitter can transmit as many packets as possible in one set up, while not exceeding the memory.
11. Random delay between each transmitted packet: min rand 1024 symbols, max rand 2048 symbols. The time period corresponds to roughly 1-2 μs.
12. Used preamble sequence: the length 31 ternary code {-0+-00+++-+000-+0+++0-0+0000-00}, whose code index is 5 [3].
13. SFD: the short SFD, which is {0+1 0 -1 +1 0 0 -1} spread by a preamble symbol.
14. PRF: 16MHz.
15. PAC: 16.
16. Width of the corridor (second scenario): 1.8m.
17. Heights of the antenna from the ground of the corridor (second scenario): 0.28m. These heights are measured by a meter. The height of an antenna is the distance between the plastic surface, where the DW1000 is located on, and the surface of the corridor's ground.

Figure 3.10. Picture of the small chamber within the anechoic chamber.

3.6.2. Measurement environment

The measurements were divided into two parts. The first part tested the performance of different preamble lengths in an anechoic chamber, with minimal multipath components. The second set of measurements was done in a straight corridor. The

surfaces of the walls and the floor were quite smooth and flat. Thus, it can be seen as an example of indoor LOS environment. There were two pervasive communications systems within the testing area: panOULU, and eduroam. So there might be interference if the two systems could overlap with our system in band [17].

In order to create an environment with as little multipath components as possible, a small chamber was built within a large anechoic chamber. The walls and the floor of the small chamber had non-reflective surfaces. The height of the walls was above 3 meters. The total length of the small chamber was about 7 meters. Fig 3.10 and Fig 3.11 show the two environments, correspondingly.

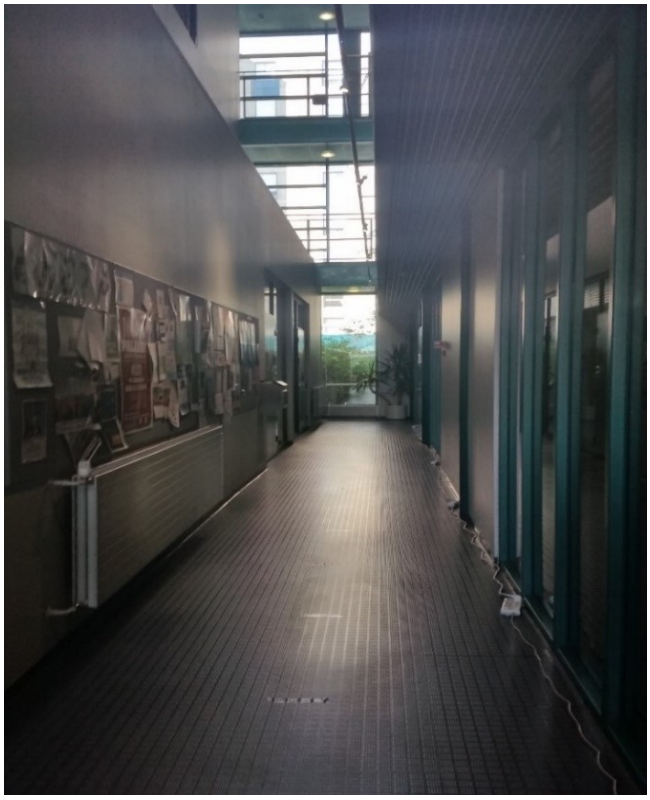

Figure 3.11. Picture of the measurement corridor.

3.6.3. Measurement steps

Each of the nodes was connected to a laptop for configuration and data collections. After a cold power-up, a configuration was performed so that the two devices could be synchronized with each other. This was done by sending small amounts of packets from one node to the other several times. After the configuration was done, the two nodes were ready for measurements. **It is necessary to point out that one laptop was the operation side, where commands for setting up the measurements and starting the tests were made. The node, which was connected to the operation side's laptop, automatically became the SINK node** [22].

First, the two devices were located at the same height. The antennas on both devices were set to point in opposite directions from each other, and the directions they pointed formed a straight line, which was parallel with the chamber or the corridor.

In both parts of the measurements, the SINK node was settled down at a certain place, and it acted as the receiver (however, the two nodes were both transmitting to and receiving from each other). The END node was moved away from the SINK. At each individual distance measurement, all the preamble lengths were tested.

The total length of the small chamber was about 7 meters. So the maximum measurement length was set to be 6 meters. At first, the distance between the END and the SINK was 1 meter. Then the distance was increased by 1 meter in steps, until it reached 6 meters.

For each tested preamble length at a specific distance, a total number of 96000 packets were transmitted to give statistically meaningful results. Since the maximum number of packets that could be sent at a time was 4000, so each measurement was repeated 24 times.

The total length of the corridor was about 16 meters. The maximum length for measurement was set as 11 meters. The SINK was positioned at the entrance of the corridor, while the END was moved towards the glass wall at the end of the corridor. The starting distance between the nodes was 1 meter. The distance was increased by 1 meter in steps, until it reached 11 meters. For each preamble length at a specific distance, a total number of 40000 packets were transmitted to give statistically meaningful results.

3.6.4. Statics to be collected

This section will introduce the statistics to be collected, and discuss the system's transmission and reception process in detail. The useful counters to be collected from Report_t file are

1. Channel Impulse Response Power (CIR_PWR):
   This is a 16-bit value reporting the sum of the squares of the magnitudes of the accumulator from the estimated highest power portion of the channel. By using the CIR_PWR and PreambleAcc, the received signal power level can be estimated by Eq. (3.2).

2. PHY Header Error (PHE):
   This event status bit is set to indicate that the receiver has found a non-correctable error in PHR. The PHR includes a SECDED error check sequence that can correct a single bit error and detect a double bit error.

3. FCS Good (FCG):
   This counter shows the number of correct receptions of the valid frames, which has passed through FCS checking.

4. FCS Error (FCE):
   The FCE is a guard against too many Reed-Solomon decoding errors (RSE). When too many RSEs occur, Reed-Solomon decoding fails completely.

5. Overrun (OVR):
   The number of overrun errors occurred in the receiver.

6. Preamble detection timeout (PTO):

This event bit is set when the preamble detection timeout occurs. The PTO occurs when the receiver is **expecting a response frame to arrive within a fixed time**, but the frame's preamble is not detected in that period [13].

7. Reed Solomon Decoder Error (RSE):
   The RSE field is a 12-bit counter of the non-correctable, but detectable error events that can occur during Reed Solomon decoding.

8. Frame Filter Rejection Event Counter (FFR):
   The FFR field is a 12-bit counter of the frames rejected by the receive frame filtering function. Once the receiver has received and decoded the MHR of a frame, it will check the address information. If the receiver finds out any error in the address information, the received frame will be aborted immediately, and the receiver will not go on to receive other parts of the frame.

9. SFD timeout errors Event Counter (STO):
   The STO field is a 12-bit counter of SFD timeout error event. The STO error occurs when the preamble has been detected, but the receiver cannot find the SFD within a fixed time duration. The STO can be a guard against the false detection of preamble.

10. TX Frame Sent Event Counter (TXFS):
    The TXFS field is a 12-bit counter of transmitted frames sent. This counter's value is incremented by one every time a frame is sent. Retransmission of a frame also increments TXFS's value.

11. Half Period Warning Event Counter (HPW):
    It is a 12-bit counter. HPW errors occur as the result of late invocation of delayed transmission or reception functionality.

12. TX power-up warning event counter (TPW):
    It is a 12-bit counter. A TPW error occurs when a delayed sent time is too short to allow proper power-up of the TX blocks, before the delayed transmission is due to start.

13. Frame Wait Time Out (FWTO):
    Each time the END node finishes transmitting a frame, it will transit into receiving mode, and wait for the ACK from the SINK node to arrive. A FWTO error occurs if the ACK frame does not arrive within a certain time duration. The FWTO errors can only occur at the END node.

14. Preamble Accumulated:
    Once a preamble is detected, the receiver begins accumulating correlated preamble symbols, while looking for the SFD sequence. Accumulation is stopped when the SFD is detected, but may stop earlier if the accumulated energy in the accumulator grows quickly, as is in the case of close line-of-sight conditions. In this case, the receiver continues receiving preamble symbols, without accumulating them, while searching for the SFD sequence.

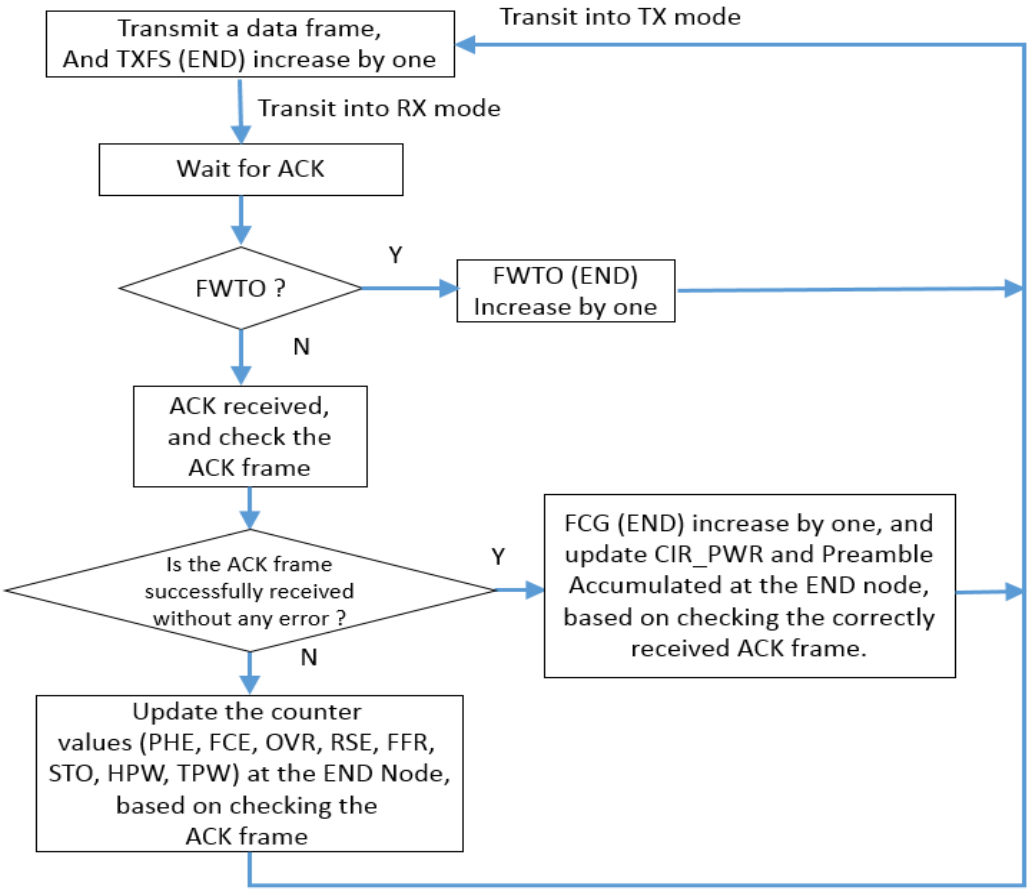

Fig 3.12. Diagram of switching states at the END node.

Fig 3.12 shows the switching states at the END node. Each time after the END node has finished transmitting a data packet to the SINK node, the TXFS(END) will increment by one, and the END node will transit into receiving mode to wait for the ACK packet from the SINK node. If the ACK packet does not arrive within a fixed time period, the END will count it as a FWTO error, and the FWTO(END) will increment by one. The END node will then move on to transmit the next data packet. Otherwise, the END node will check the received ACK packet for possible errors. All the counters' values at the END node (except FWTO and TXFS) are counted based on checking the received ACK packet. The difference between a data packet and an ACK packet is that an ACK packet does not contain any data payload.

Fig 3.13 shows the stitching states at the SINK node. At the SINK node's side, the preamble accumulation will begin, once the SINK node has detected a preamble of the data packet. All the counters' values at the SINK node (except TXFS) are counted based on checking the received data packet. The SINK node will only send the ACK packet back, based on the FCG of the received data packet. After the SINK node sends the ACK packet back to the END node, the TXFS(SINK) will increment by one, and the SINK node will transit into receiving mode again.

In our measurements setting, the SINK node actually begins transmission of the ACK packet at about 6 to 8 μs after reception of the last data packet bit. However, the END node is ready to receive the ACK packet only after 10 μs since finishing transmitting the data packet.

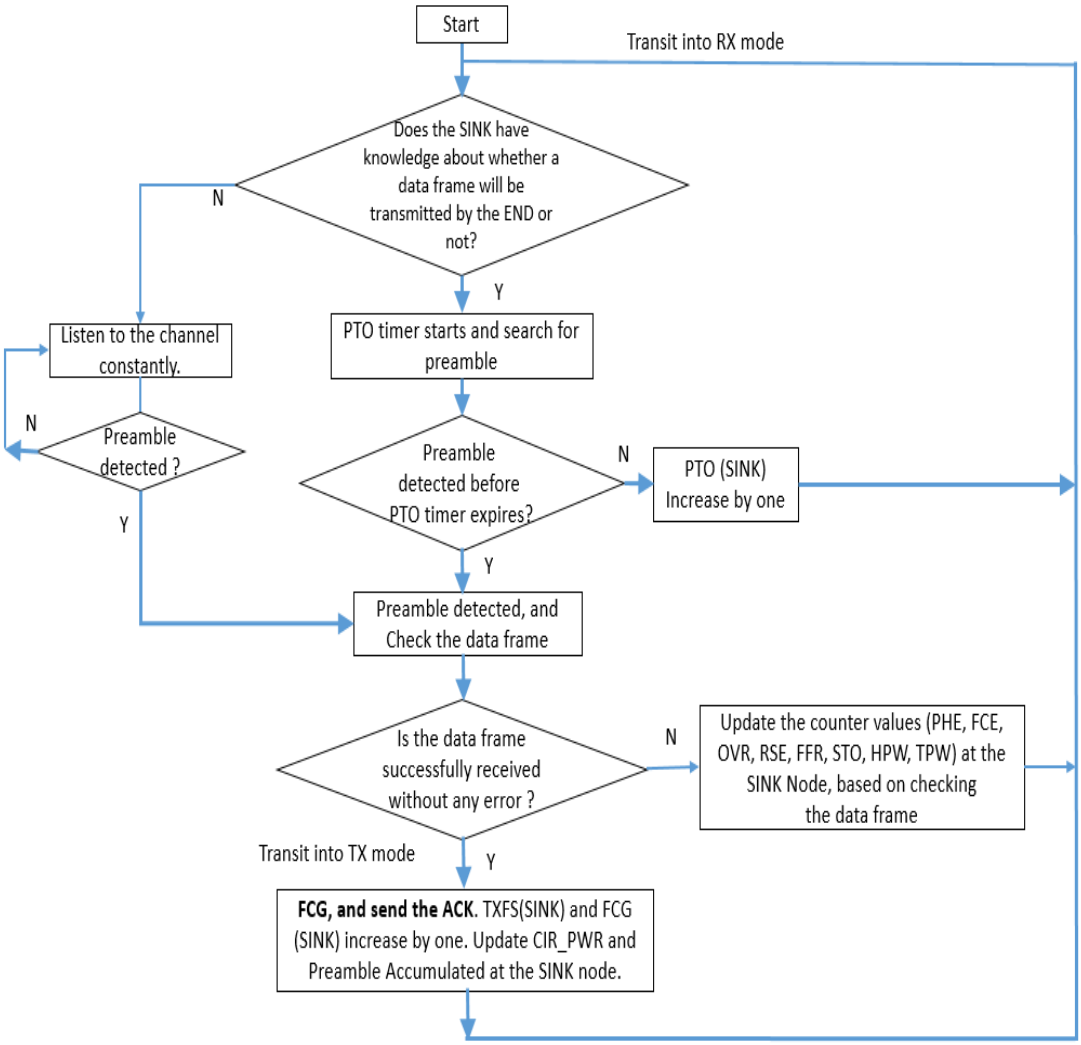

Fig 3.13. Diagram of the switching states at the SINK node.

3.7. Theoretical predictions on the results

Previously, we have discussed all the necessary information about the measurements. In this section, theoretical predictions will be made before the results, which will help further analyzing data more easily.

Before moving on to predicting the results of measurements under two scenarios, the most important factors, that will affect analysis method directly, will be discussed at first.

3.7.1. Possible factors affecting results and analogy

In the measurements of first scenario, there is no possibility for MUI, and interference from other systems. Since multipath components are almost nonexistent, the effect of multipath propagation can be neglected in the first scenario. However, in the second scenario, the devices are exposed to a real-life environment.

First, MUI in the second scenario is impossible, since there are only two devices within the testing range. According to [25, 26] and [28], neither panOULU nor

eduroam system overlaps with our system's band. More importantly, they are all narrow-band systems, and their effects are all filtered by the hardware. Thus, interference from other systems should not be possible. Due to low duty cycle, ISI would only occur when a signal from a different path can travel more than half of a data symbol's period to cause it. That means a different path has to be 150 meters longer. For the preamble part, the duration of each preamble code is 16 chips, which corresponds to 9.6m. In the second scenario environment, it is geometrically impossible for a different path, which is only reflected once, to be 9.6 meters longer than the direct path. If we consider that a signal is reflected multiple times to reach the receiver, the signal power left is too small to have an effect. From the analysis above, the only factor left to affect the analogy in the second scenario is the multipath propagation.

3.7.2. Analysis and predictions on the second scenario's measurements

In this part, the analyzing method, which is based upon different UWB multipath propagation channel models, will be discussed at first. Then the predictions on the results of second scenario's measurements will be given.

3.7.2.1. Analogy of the second scenario's measurements

Chapter 2 introduced three multipath propagation UWB channel models. The SK and SBY model will be omitted here. The S-V model points out that in the real UWB channel, different multipath components arrive in clusters, and the arrival time of those clusters is undetermined [31, 32, 33]. The S-V model also describes the channel as block fading.

The S-V model can perfectly describe a NLOS environment. However, it is not precise in describing LOS environments [32]. This is due to the fact that in NLOS environment, there are many reflecting factors. In a LOS environment, such factors are much fewer. Thus, the clusters will be more deterministic. Various reports show that in a LOS environment at short ranges, the path loss of the channel will suddenly increase and then decrease [32]. This phenomenon of a sudden change in the path loss at a certain distance is quite similar to that of a narrowband system.

Thus, the two-ray ground reflection model will be employed to give a coarse estimation on the distance, where the sudden increase in path loss may appear. On the other hand, the channel is still regarded as **block fading**.

3.7.2.2. Predictions on the results of the second scenario's measurements

In the second scenario, the purpose of measurements is to find how differently the system will perform in both environments with minimal multipath components and rich multipath components. All the common factors that a multipath propagation scenario inherits from a non-multipath propagation scenario will be skipped.

1. Received signal power:
   IEEE 802.15.4-2011 UWB standard [5] can allow ED receiver to take advantage of multipath propagation, in the way of collecting more energy from

peaks of multipath components. Thus, the received signal power level of second scenario is naturally higher than that of the first scenario. Since the power of the preamble is increased as well, synchronization performance will become better. This leads to an enhanced performance of packets reception.

2. Effects of block fading on different parts of the frame:
   In a block fading channel, the channel impulse response changes over time. When it changes, the change will last over approximately one symbol duration, and stays constant over that duration. The duration between each change is an expected value, which also known as 'block size'. When distance increases in corridor, the block size will become smaller, due to more complexity in channel.

   When block fading happens, it may corrupt a preamble symbol or a data symbol. The corruption of preamble symbols can decrease the number of accumulated preamble symbols. On the other hand, the increase in SNR will result in more preamble symbols to be accumulated, which might compensate for the decrease.

   Based on previous discussion, RS encoding is robust towards consecutive burst errors, but it is rather weak towards sparsely distributed errors. The block fading errors can be regarded as sparse and unpredictable. Thus, the block fading might increase the RSE. However, the increase in SNR will also decrease the RSE, which might compensate for the increase in RSE.

3. 'Breaking point' estimation:
   By implementing Eq. (2.20), the corresponding breaking point distance in our test is approximately 4.7m. The distance between the antenna and the ground of the corridor is 0.28m, which is much shorter than the distance between the antenna and the corridor walls (approximately 0.9m).

4. Block fading causing instability:
   Regarding a cold start up, where the two devices are totally unsynchronized. They will need a certain number of tries to get synchronized, and stably send packets to each other.

   In block fading channel, there may be a similar 'cold start up' effect, caused by channel impulse response changing within the period of time, where two devices are not synchronized. More specifically, this period should be the random delay between each data frame. In this period, if too many channel impulse response changes take place, the two devices will become unsynchronized with each other, just like it is in the case of a cold start up.

   Suggest that a number of N block fading channel responses are expected to take place within a random delay period. If distance increases, the environment will get more complicated, which will cause the block size to become smaller. Also, if the random delay duration gets longer, it would allow more block fading channel impulse responses to take place. The longer preamble lengths have better synchronization performance than the shorter preamble lengths, thus a longer preamble length can endure more changes of block fading channel impulse responses, and can offer a longer operating distance.

4. Results and analysis

In this chapter, the results of the first and the second scenario measurements are presented. Analysis will be given, based on these results. The theoretical predictions in the previous chapter will also be tested.

4.1. Results and analysis of the first scenario measurements

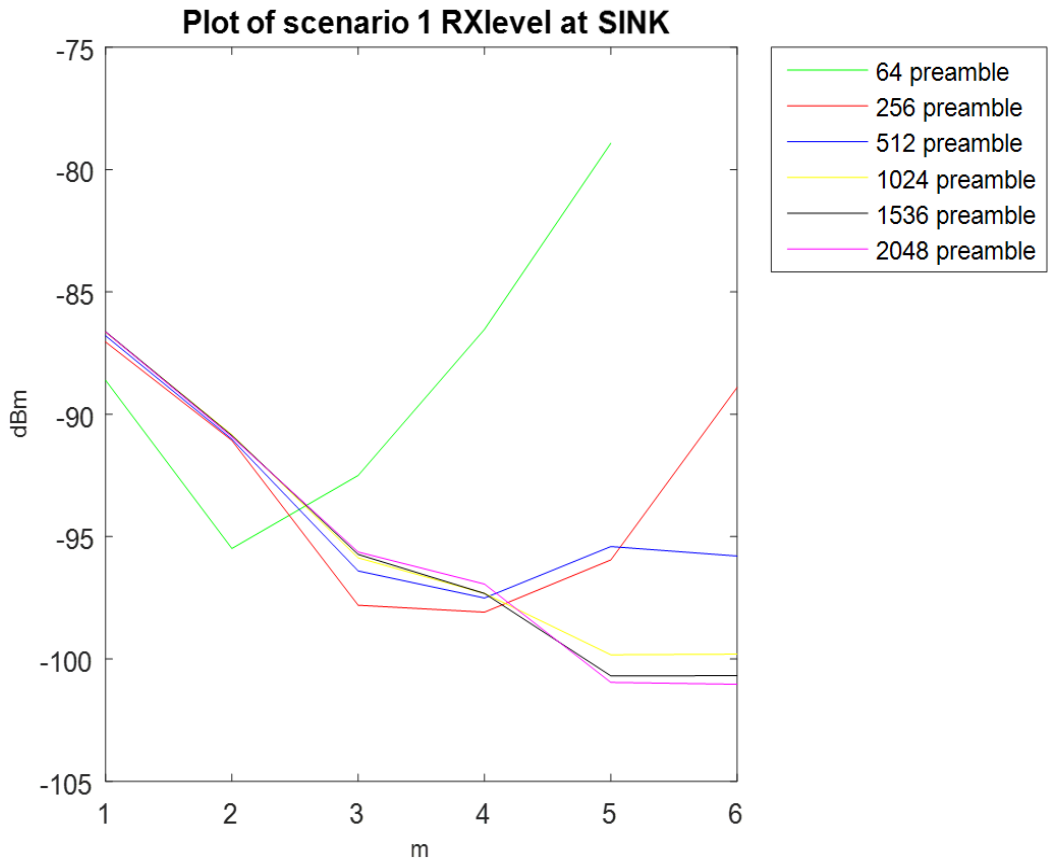

Figure 4.1. Diagram of the first scenario's received signal powers at the data frame.

Fig 4.1 shows the received signal powers of different preambles in scenario one at SINK. It should be a general trend for the received signal power to drop, as the distance increased. However, both the 64 preamble length and the 256 preamble length have reverse trends when the distances are long. However, for the 256 preamble length, the received signal power starts to sharply increase at 5m, while for the 64 preamble length, the received signal power sharply increases at 3m. This is probably caused by receiver significantly increasing the AGC for detecting the 64 preamble length and the 256 preamble length at long distances. Another explanation could be that as only a fraction of the transmitted frames are received, their received signal strength is higher due to the random fluctuation of the channel.

Fig 4.2 shows the received signal power of different preambles at the END. By comparing Fig 4.2 with Fig 4.1, we can find out that for most preamble lengths, the ACK frames' received signal power level is very close to that of the data frames' at

the same distance. Only in the 64 preamble length's case, the ACK frames' received signal power level is quite different from that of the data frames' at each location.

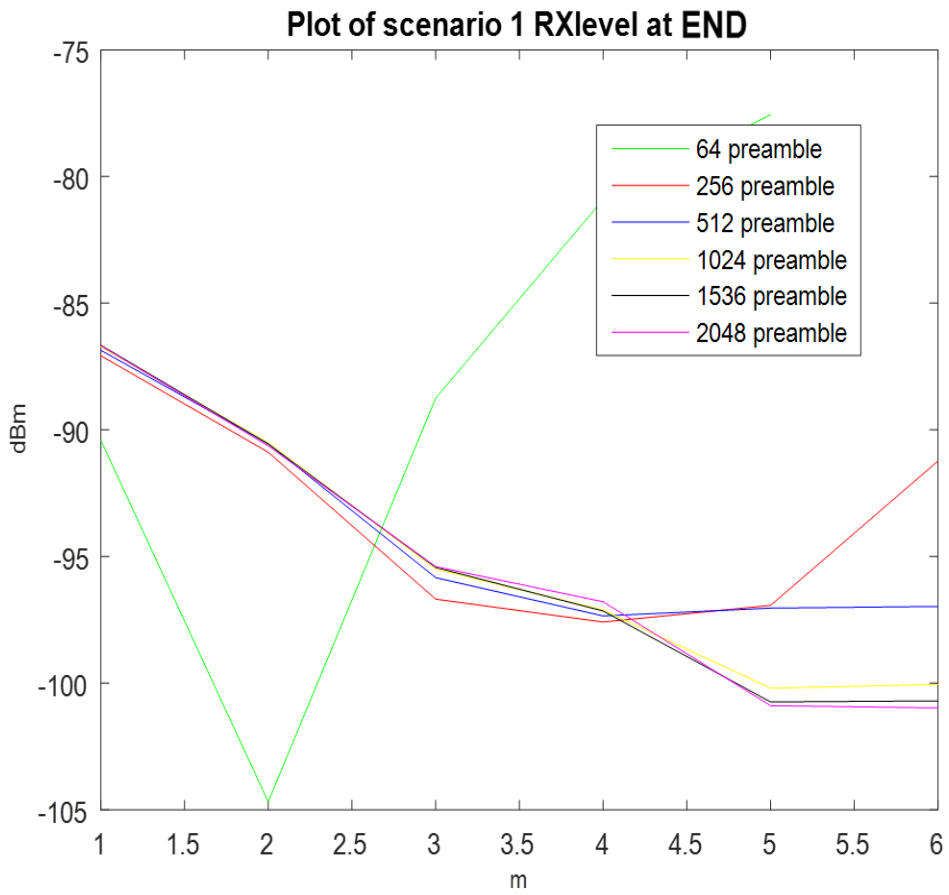

Figure 4.2. Diagram of the first scenario's received powers at the ACK frame.

Table 4.1 shows the counters' values of 64 preamble length. **Throughout the whole measurements**, the PTO, OVR, HPW, and TPW counters all have the values of zeros. Thus, they will not be listed in any of the counters' tables. In addition to all the necessary counters, **four** other counters are introduced as well. They will also be utilized throughout other preamble lengths' tables.

MP stands for missing packets. It is shown in Table 4.1 that, if all the counter values of 5m(SINK) are added up, the sum does not equal 4000. This means that some data frame packets are failed to be detected by the SINK node. On the other hand, if all the counter values (except FWTO) of 5m(END) are added up, the sum does not equal 1675. This means that some ACK frame packets are also failed to be detected by the END. However, the ACK frame packets, which are failed to be detected by the END, are counted as FWTOs.

The missing packets are most likely to be caused by failure of detecting the preamble, or in other words, any preamble symbol. If the receiver can detect at least one preamble symbol, the receiver will go on to detect other parts of the packet, and the packet will not be missing.

The reason, why the missing packets are not counted as PTOs, is probably because when the receiver has no knowledge of whether there will be any more packet to come

up, **it will not listen in response to search for the preamble**. In this situation, if the receiver fails to detect any preamble symbol in a period of time, the packet will be directly missed, instead of being counted as a PTO.

MPR stands for the missing packets rate. The MPR can reflect the detectability of each preamble symbol within a certain preamble length. A smaller MPR would mean that the detectability of each preamble symbol is good. It is necessary to point out that the MPR is only used for comparison within the same preamble length. Since a long preamble length naturally has a lower probability for the receiver to miss detecting any of the its preamble symbol, a lower MPR of a long preamble length cannot indicate that its detectability of a single preamble symbol is better than that of a short preamble length, with a higher MPR. Equations (4.1) and (4.2) define the MPR for both the data and the ACK packets as

$$\mathrm{MPR(data)} = \frac{MP(SINK)}{TXFS(END)}, \tag{4.1}$$

$$\mathrm{MPR(ACK)} = \frac{MP(END)}{TXFS(SINK)}. \tag{4.2}$$

STOR stands for the STO rate. It had been mentioned earlier that STO is a guard against any false detection of the preamble. However, there are other reasons for STO to occur. First, a corrupted SFD part will cause the STO. Second, the receiver might listen into the SFD, and still regard it as a part of the preamble and consequently miss the SFD. In general, the STOR can also reflect the detectability of each preamble symbol in some extent. Like the MPR, the STOR is also only used for comparison within the same preamble length. Equations (4.3) and (4.4) define the STOR for both the data and the ACK packets as

$$\mathrm{STOR(data)} = \frac{STO(SINK)}{TXFS(END)}, \tag{4.3}$$

$$\mathrm{STOR(ACK)} = \frac{STO(END)}{TXFS(SINK)}. \tag{4.4}$$

PRR stands for packets being received rate, and it is the rate of FCG. The PRR can be used as an indicator for the overall packet receiving performance. Equations (4.5) and (4.6) define the PRR for both the data and the ACK packets as

$$\mathrm{PRR(data)} = \frac{FCG(SINK)}{TXFS(END)}, \tag{4.5}$$

$$\mathrm{PRR(ACK)} = \frac{FCG(END)}{TXFS(SINK)}. \tag{4.6}$$

It can be seen from Table 4.1 that PRR (data frame) is always higher than PRR (ACK frame) within the distance of 4m. It is natural to suggest that the ACK frames should have better synchronization than the data frames at each distance. Thus, the ACK frames' overall performance should be better than that of the SINK at each distance. However, this suggestion does not fit into the 64 preamble length's situation.

From Table 4.1, we can see that the MPR (data frame) is always higher, or equal to, the MPR (ACK frame) at each distance. Also, the STOR is always zero. This suggest that, for the 64 preamble length, the detectability of a single preamble symbol is better in the ACK frames than in the data frames.

Table 4.1. Counters of the 64 preamble length

	1m END	1m SINK	2m END	2m SINK	3m END	3m SINK	4m END	4m SINK	5m END	5m SINK
PHE	82	3	89	4	303	232	568	425	505	719
RSE	100	39	108	46	159	189	184	269	137	369
FCG	3532	3957	3502	3948	2795	3565	2141	3222	722	1675
FCE	2	0	3	0	4	0	5	0	4	1
FFR	234	2	247	2	305	14	306	25	186	42
STO	0	0	0	0	0	0	0	0	0	1
FWTO	44	0	52	0	436	0	797	0	2446	0
TXFS	4000	3957	4000	3948	4000	3565	4000	3222	4000	1675
MP	7	0	0	0	0	0	18	59	121	1193
MPR	0.18%	0	0	0	0	0	0.56%	1.5%	7.2%	30%
STOR	0	0	0	0	0	0	0	0	0	0
PRR	89%	99%	89%	99%	78%	89%	66%	81%	42%	41%

Fig 4.3 shows the preamble accumulated number of the 64 preamble length. Within the 5m's working range, the SINK node always can accumulate more preamble symbols at each distance. The number of accumulated preamble symbols at the SINK node drops smoothly as the distance increases. However, the number of accumulated preamble symbols of the 64 preamble length remains quite constant at each distance.

Table 4.2 shows the counters' values of 256 preamble length. The MP number becomes apparently large at 6m, and there is no missing packet within 5m's distance. At 6m, the MPR is much higher for the data packets than for the ACK packets. At 6m, the STOR is also higher for the data packets than for the ACK packets. Both the MPR and the STOR suggest that for the 256 preamble length, the ACK packets have better detectability of preamble symbol than the data packets at long distances.

It can be seen from Table 4.2 that the overall packets receiving performance of the ACK packets is slightly better than that of the data packets' at each distance. This might indicate that the ACK packets have better synchronization than the data packets for the 256 preamble length.

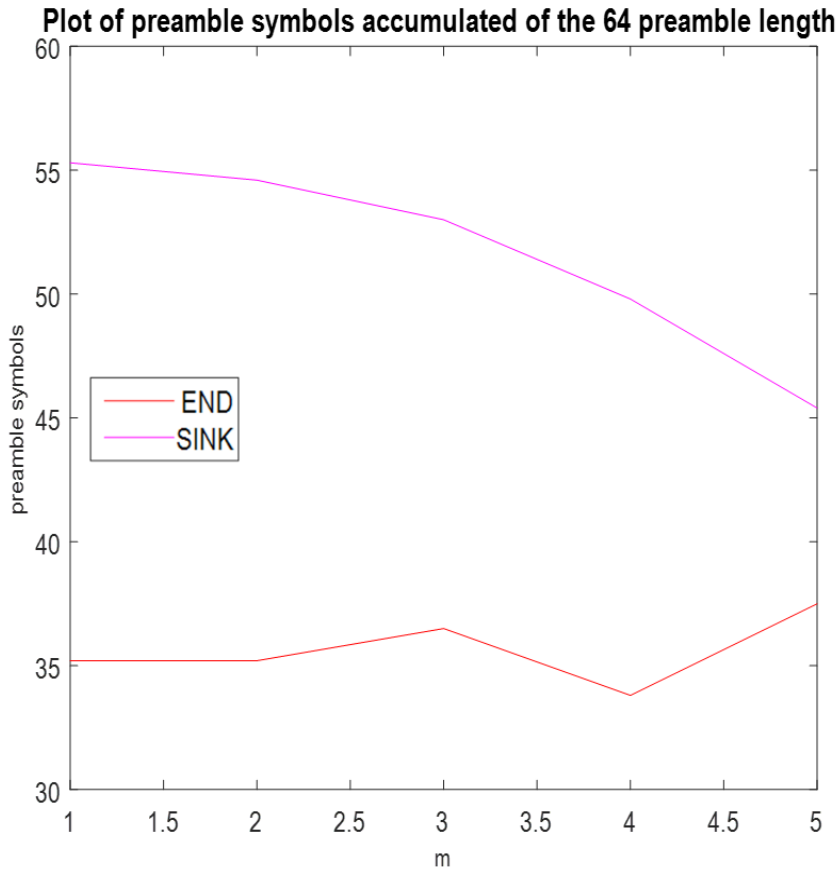

Figure 4.3. Graph of the 64 preamble length's PreambleACC.

Table 4.2. Counters of the 256 preamble length

	1m END	1m SINK	2m END	2m SINK	3m END	3m SINK	4m END	4m SINK	5m END	5m SINK	6m END	6m SINK
PHE	0	0	0	0	86	93	177	208	402	500	553	897
RSE	0	0	0	0	9	11	20	24	44	58	77	164
FCG	4000	4000	4000	4000	3792	3892	3554	3759	2949	3416	1172	2070
FCE	0	0	0	0	0	0	0	0	1	1	2	2
FFR	0	0	0	0	4	4	8	9	21	25	62	48
STO	0	0	0	0	0	0	0	0	0	0	10	56
FWTO	0	0	0.16	0	108	0	241	0	584	0	2125	0
TXFS	4000	4000	4000	4000	4000	3892	4000	3759	4000	3416	4000	2070
MP	0	0	0	0	1	0	0	0	0	0	194	763
MPR	0	0	0	0	0	0	0	0	0	0	9.4%	19.1 %
STOR	0	0	0	0	0	0	0	0	0	0	0.5%	1.4%
PRR	100 %	100 %	100 %	100 %	97.4 %	97.3 %	94.5 %	94%	86.3 %	85.4 %	56.6 %	51.8 %

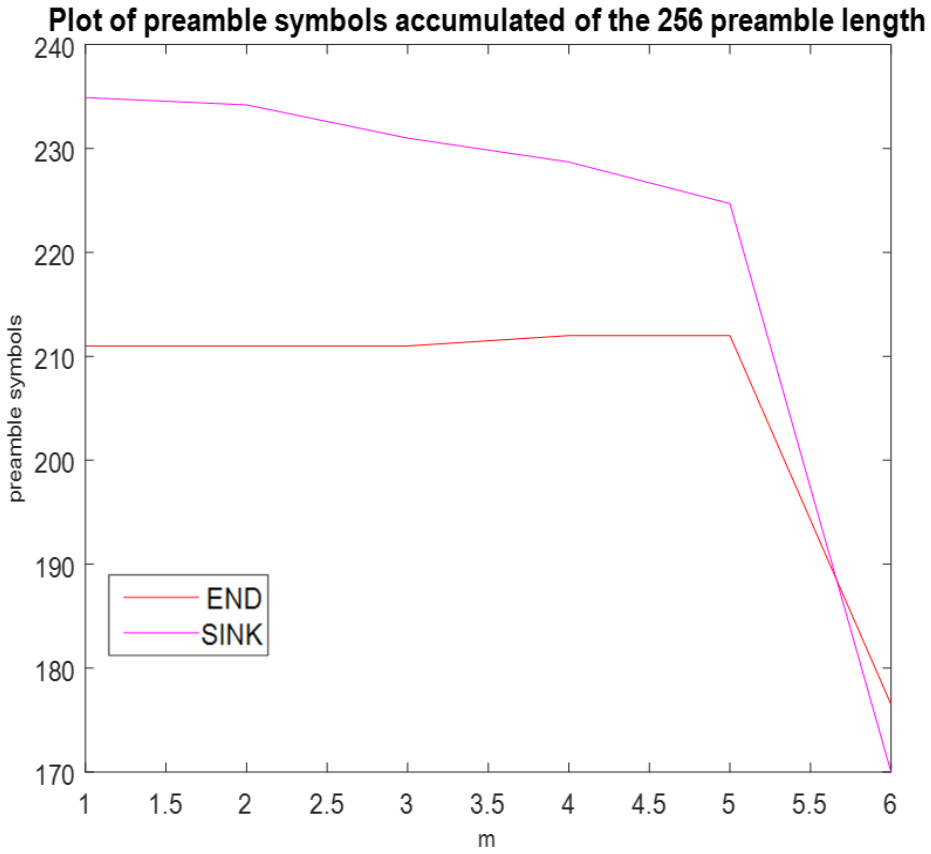

Figure 4.4. Graph of the 256 preamble length's PreambleACC.

Fig 4.4 shows the accumulated preamble symbols of the 256 preamble length. We can see that the data packets can accumulate more preamble symbols within the distance of 5m. However, the number of accumulated preamble symbols drops a lot for both the data packets and the ACK packets at 6m. And the data packets have a sharper drop in the number of accumulated preamble symbols than the ACK packets. This might be related to the STOR and MPR values becoming apparently large at 6m in Table 4.2.

It is natural to suggest that the sudden rise in the number of MP and STO means that the detectability of preamble symbol fails dramatically. Thus, the number of accumulated preamble symbols drops sharply. Since the data packets' MPR and STOR are larger at 6m, the number of accumulated preamble symbols drops sharper for the data packets at 6m. In addition, the 64 preamble length's case can also prove this. The data packets' MPR is higher than that of the ACK packets' for the 64 preamble length. In Fig 4.3, we can see that the ACK packets' accumulated preamble symbols number does not drop as much as that of the data packets' throughout the 5 meters' distance.

Table 4.3. Counters of the 512 preamble length

	1m END	1m SINK	2m END	2m SINK	3m END	3m SINK	4m END	4m SINK	5m END	5m SINK	6m END	6m SINK
PHE	0	0	0	0	81	82	187	216	647	995	639	938

RSE	0	0	0	0	9	10	21	27	75	124	75	112
FCG	4000	4000	4000	4000	3810	3904	3531	3749	1813	2632	1956	2750
FCE	0	0	0	0	0	0	0	0	0	2	1	1
FFR	0	0	0	0	4	3	10	8	41	47	37	47
STO	0	0	0	0	0	0	0	0	13	61	10	57
FWTO	0	0	0	0	96	0	251	0	1412	0	1281	0
TXFS	4000	4000	4000	4000	4000	3904	4000	3749	4000	2632	4000	2750
MP	0	0	0	0	0	1	0	0	43	139	32	95
MPR	0	0	0	0	0	0	0	0	1.6%	3.5%	1.2%	2.4%
STOR	0	0	0	0	0	0	0	0	0.5%	1.5%	0.4%	1.4%
PRR	100 %	100 %	100 %	100 %	97.6 %	97.6 %	94.2 %	93.7 %	68.9 %	65.8 %	71.1 %	68.8 %

Table 4.3 shows the counters' values of 512 preamble length. MP becomes apparently large for both the ACK packets and the data packets when the distance reaches 5m. The data packets have a larger MPR. The STOR of the data packets is also higher than that of the ACK packets'. Thus, for the 512 preamble length, the ACK packets have better detectability of preamble symbol than the data packets. It can be seen from Table 4.3 that the overall performance of the ACK packets is slightly better than that of the data packets'.

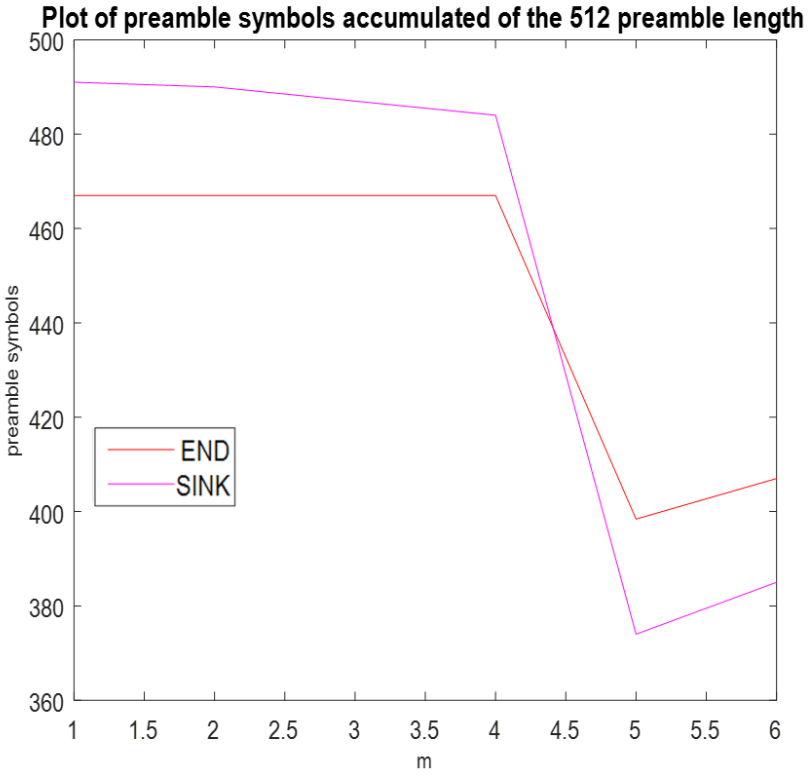

Figure 4.5. Graph of the 512 preamble length's PreambleACC.

Fig 4.5 shows the number of accumulated preamble symbols of 512 preamble length. It can be seen from Fig 4.5 that the data packets can accumulate more preamble symbols than the ACK packets within 4m's distance. When the distance is beyond 4m, the ACK packets accumulate more preamble symbols than the data packets. The sharp drop in the number of preamble symbols accumulation also takes place in the 512 preamble length's case. The data packets have larger MPR and STOR, and its preamble symbol accumulation number drops more sharply.

Table 4.4. Counters of the 1024 preamble length

	1m END	1m SINK	2m END	2m SINK	3m END	3m SINK	4m END	4m SINK	5m END	5m SINK	6m END	6m SINK
PHE	0	0	0	0	77	79	193	215	668	1023	649	958
RSE	0	0	0	0	11	10	21	26	73	115	71	106
FCG	4000	4000	4000	4000	3817	3908	3527	3750	1949	2750	2059	2830
FCE	0	0	0	0	0	0	0	0	1	1	1	1
FFR	0	0	0	0	4	3	9	9	37	50	32	50
STO	0	0	0	0	0	0	0	0	14	61	13	55
FWTO	0	0	0	0	92	0	250	0	1258	0	1176	0
TXFS	4000	4000	4000	4000	4000	3908	4000	3750	4000	2750	4000	2830
MP	0	0	0	0	0	0	0	0	8	0	5	0
MPR	0	0	0	0	0	0	0	0	0.3%	0	0.2%	0
STOR	0	0	0	0	0	0	0	0	0.5%	1.5%	0.5%	1.4%
PRR	100%	100%	100%	100%	97.7%	97.7%	94.1%	93.8%	70.9%	68.8%	72.8%	70.8%

Table 4.4 shows the counters' values of 1024 preamble length. The MP values of the Table 4.4 are quite different from those of the previous tables. It can be seen from Table 4.4 that there are no missing packets at the SINK node. The numbers of missing packets are quite small at the END node. This would suggest that the 1024 preamble length is already long enough to eliminate the chance of miss detecting all the preamble symbols. However, the missing packets of the ACK packets might be caused by some unknown reasons.

The STOR of the data packets is higher than that of the ACK packets'. The overall performance of the ACK packets is slightly better than that of the data packets'.

Fig 4.6 shows the number of accumulated preamble symbols of 1024 preamble length. It can be seen from Fig 4.6 that within 2m, the number of accumulated preamble symbols at both nodes rises as the distance increases. This is because, when the distance is too short, the energy in accumulator grows too fast, and the accumulator stops accumulating.

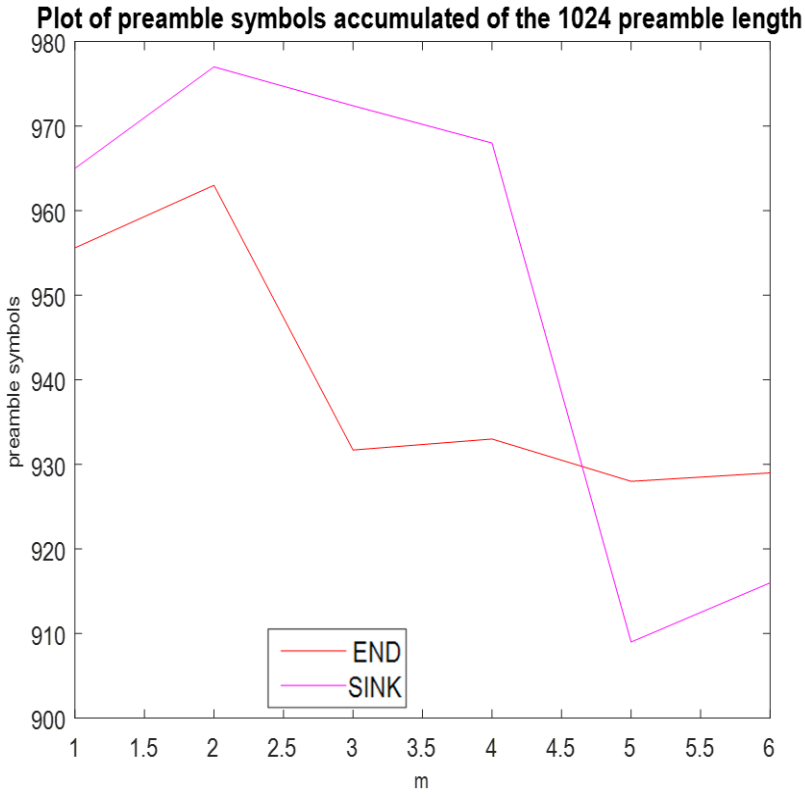

Figure 4.6. Graph of the 1024 preamble length's PreambleACC.

Within 4m's distance, the data packets can accumulate more preamble symbols than the ACK packets. However, the data packets' accumulated preamble symbols' number sharply decreases at 5m, while the ACK packets' accumulated preamble symbols' number remains quite constant. The ACK packets' accumulated preamble symbols' number has a drop at 3m, and there are no missing packets or STOs. Thus, the drop at 3m might be caused by some unknown reasons. In the 1024 preamble length' case, it is hard to tell whether the data packets or the ACK packets have better detectability of preamble symbol.

Table 4.5. Counters of the 1536 preamble length

	1m END	1m SINK	2m END	2m SINK	3m END	3m SINK	4m END	4m SINK	5m END	5m SINK	6m END	6m SINK
PHE	0	0	0	0	81	82	200	236	657	1015	670	987
RSE	0	0	0	0	9	10	24	27	73	117	72	112
FCG	4000	4000	4000	4000	3811	3904	3493	3727	1983	2770	2000	2798
FCE	0	0	0	0	0	0	0	0	0	2	1	2
FFR	0	0	0	0	4	4	10	10	36	48	34	49
STO	0	0	0	0	0	0	0	0	0	48	0	53
FWTO	0	0	0	0	96	0	273	0	1250	0	1222	0

TXFS	4000	4000	4000	4000	4000	3904	4000	3727	4000	2770	4000	2798
MP	0	0	0	0	0	0	0	0	21	0	21	0
MPR	0	0	0	0	0	0	0	0	0.8%	0	0.8%	0
STOR	0	0	0	0	0	0	0	0	0	1.2%	0	1.3%
PRR	100 %	100 %	100 %	100 %	97.6 %	97.6 %	93.7 %	93.2 %	71.6 %	69.3 %	71.5 %	70%

Table 4.5 shows the counters' values of the 1536 preamble symbol length. The data packets have no missing packets. This would suggest that the 1536 is long enough, so that the receiver will not miss detecting all the preamble symbols. However, the ACK packets have missing packets at 5m and 6m. Like the 1024 preamble length, this might be caused by some unknown reasons.

On the other hand, the ACK packets have no STOs. The overall performance of the ACK packets is slightly better than the data packets.

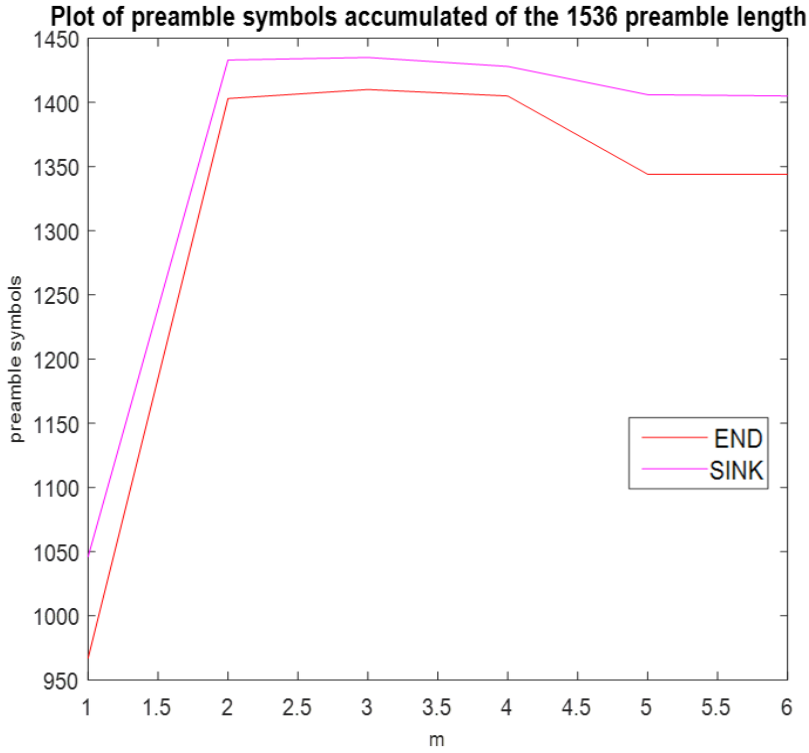

Figure 4.7. Graph of the 1536 preamble length's PreambleACC.

Fig 4.7 shows the number of accumulated preamble symbols of the 1536 preamble length. The sharp rise in the number of accumulated preamble symbol from 0m to 2m is because the accumulator stops accumulating when the distance is too short.

It can be seen from Fig 4.7 that the data packets always accumulate more preamble symbols than the ACK packets. Both the ACK packets and the data packets have drops in the numbers of the accumulated preamble symbols at 5m. However, the ACK packets have a sharper drop than the data packets.

From Table 4.5, we can see that the MPRs (ACK packets) are slightly higher than the MPRs (data packets) at 5m and 6m. Also from Fig 4.7, we can see that the number of accumulated preamble symbols drops slightly sharper from 4m to 5m in the ACK packets' case. These two facts would suggest that in the 1536 preamble length's scenario, the detectability of preamble symbol and synchronization ability are slightly better for the data packets than for the ACK packets at long distances.

Fig 4.8 shows the number of accumulated preamble symbols of the 2048 preamble length. The number of accumulated preamble symbols of the 2048 preamble length has a similar trend with that of the 1536 preamble length. Fig 4.8 also suggests that in the 2048 preamble length's case, the data packets have slightly better detectability of preamble symbol and synchronization ability than the ACK packets at long distances.

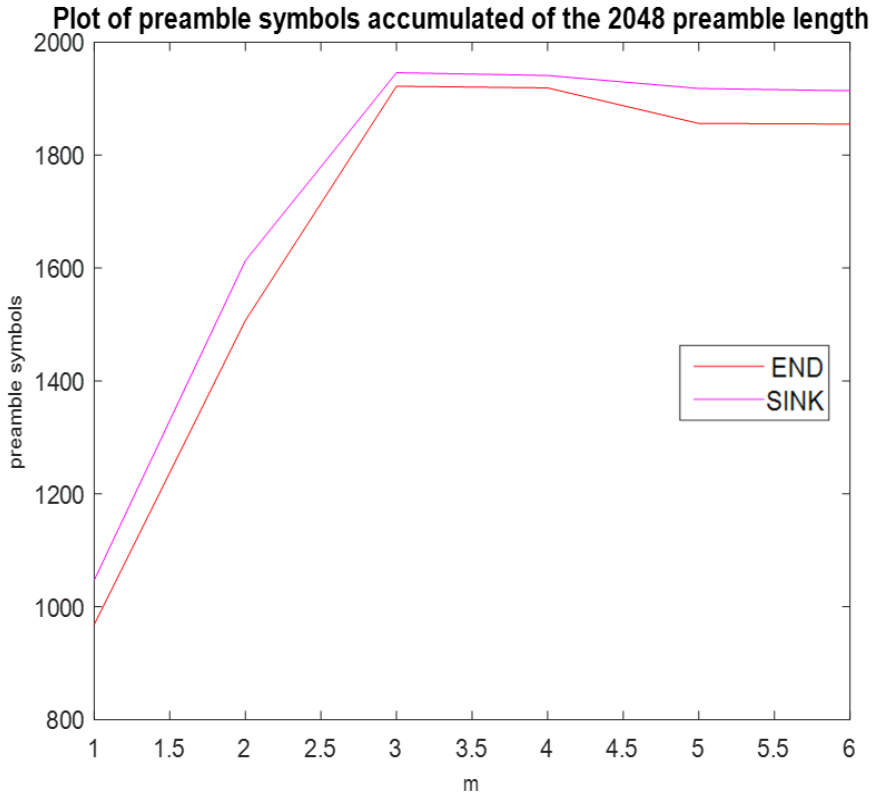

Figure 4.8. Graph of the 2048 preamble length's PreambleACC.

Table 4.6 shows the counters' values of the 2048 preamble length. It is quite like the situation in the 1536 preamble length. We can regard both the 1536 and the 2048 preamble length as 'typical' long preambles.

Table 4.6. Counters of the 2048 preamble length

	1m END	1m SINK	2m END	2m SINK	3m END	3m SINK	4m END	4m SINK	5m END	5m SINK	6m END	6m SINK
PHE	0	0	0	1	83	87	173	207	690	1057	705	1071

RSE	0	0	0	0	10	10	19	26	75	120	75	121
FCG	4000	4000	3999	3999	3803	3899	3558	3759	1902	2722	1854	2693
FCE	0	0	0	0	0	0	0	0	1	2	1	1
FFR	0	0	0	0	4	4	9	8	37	53	36	55
STO	0	0	0	0	0	0	0	0	0	46	0	60
FWTO	0	0	1	0	101	0	241	0	1296	0	1329	0
TXFS	4000	4000	4000	3999	4000	3899	4000	3759	4000	2722	4000	2693
MP	0	0	0	0	0	0	0	0	17	0	22	0
MPR	0	0	0	0	0	0	0	0	0.6%	0	0.8%	0
STOR	0	0	0	0	0	0	0	0	0	1.2%	0	1.5%
PRR	100 %	100%	100 %	100%	97.5 %	97.5 %	94.7 %	94%	70%	68.1 %	68.9 %	67.3 %

4.1.1. Conclusions on the results of the first scenario's measurements

Based upon the results and analysis above, the conclusions for the first scenario's measurements are

1. For the 64 preamble length, the data packets have better overall performance than the ACK packets at most distances. For the rest preamble lengths, the ACK packets have slightly better overall performance than the data packets. Within 4m's range, each preamble length's overall performance is quite close to that of the other preamble length's, except for the 64 preamble length. At the distance of 5m, the 256 preamble length has the best overall performance among all the preamble lengths.

2. For all the preamble lengths, the data packets can always accumulate more preamble symbols than the ACK packets at short distances. It had been mentioned earlier that the ACK transmitter actually begins transmission of the ACK at about 6 to 8 μs after reception of the last data frame bit. However, the ACK receiver is ready to receive only after 10 μs since finishing transmitting the data frame. Consequently, there is a deterministic period where ACK preamble symbols are being transmitted, but the receiver is not ready to receive them. This creates a near constant difference in the amount of the accumulated preamble symbols when the SNR is sufficient. When distance grows, other factors start to impact reception.

3. For 64, 256, and 512 preamble lengths, the ACK packets have better detectability of preamble symbol than the data packets when the distance is very long (surpasses a certain limit). This is probably because at very long distances, the signal power is rather weak, and the receiver fails to detect some of the transmitted preamble symbols. Since the ACK packets have better synchronization, the preamble symbols of the ACK packets are easier to be detected than those of the data packets'.

4. For 1536 and 2048 preamble lengths, the data packets have slightly better detectability of preamble symbol and synchronization ability than the ACK packets when the distance is very long (surpasses a certain limit). Unlike the short preamble lengths, the synchronization ability of long preambles is naturally good at long distances. Thus, both the ACK and the data packets' preamble symbols are all rather easy to be detected. However, when the preamble length gets too long, the ACK packets might have small synchronization problem or preamble symbol detecting problem.

4.2. Results and analysis of the second scenario's measurements

In this section, the results of the measurements in the second scenario are shown and analyzed. The 64 preamble length's performance is quite different from the other preamble lengths' performance. Thus the analysis of the 64 preamble length will be shown in the last part of this section. The main purpose of this part is to find out how the system performs differently in a block fading channel with multipath components. Thus, all the common characteristics with the results of the first scenario will be only discussed briefly.

Fig 4.9 shows the received signal power level at the SINK. It is clearly shown in the figure that there is a sharp drop-and-rise in received signal power at 6m. This value is quite close the one, which is 4.7m, of the coarse estimation by using two-ray ground reflection model. The general received power level is higher than that of the first scenario. This can prove that the ED receiver in the DW1000 can take advantage of multipath propagation, by accumulating more energy from the multipath components. In the LOS environment, receiving power of the signal is always sufficient.

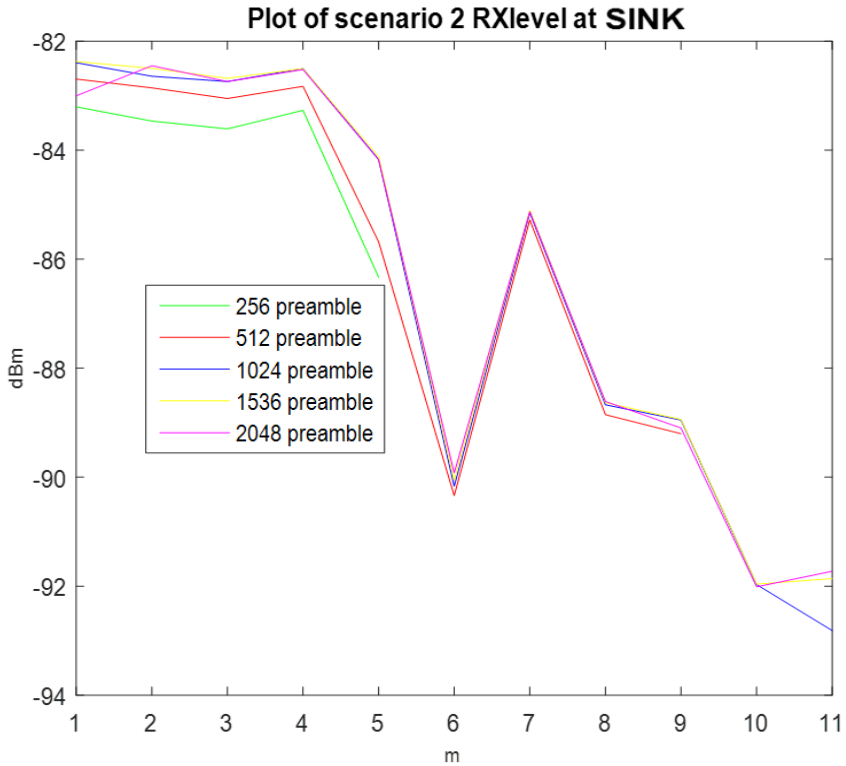

Figure 4.9. Graph of the second scenario's received signal power at the SINK.

Fig 4.10 shows the received signal power level of the END. By comparing Fig 4.9 and Fig 4.10, we can find out that the received signal power levels in both the SINK and the END are almost the same.

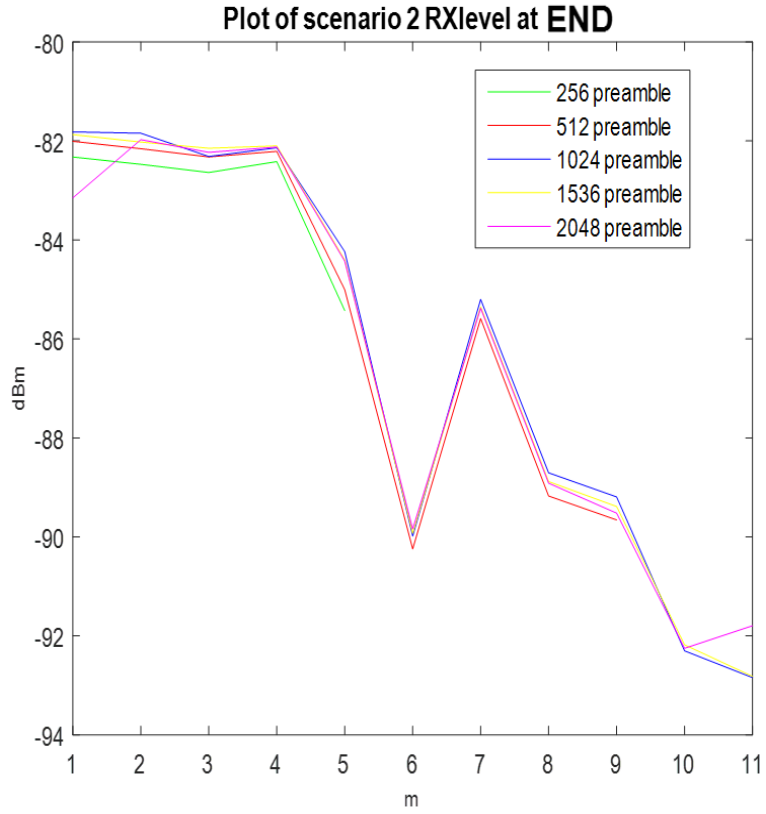

Figure 4.10. Graph of the second scenario's received signal power at the END.

Fig 4.11 shows the number of preamble symbols being accumulated at the SINK. It can be seen that the number of preamble symbols being accumulated for the 256, 512, and 1024 preamble lengths stay constant when distance increases. Based on previous analysis, the number of preamble accumulated is dependent on SNR and synchronization performance. The effect of block fading will also be considered here. In this case, the received signal power is always sufficient. The block size of the block fading channel is an expected value, which means a static amount of channel impulse responses would occur in a certain time period. This suggests that the synchronization performance should be stable and constant as well. The multipath components actually aid synchronization, in a way of offering sufficient energy to each pulse duration within the preamble part.

The sharp rise-and-drops of the 1536 and the 2048 preamble lengths are caused by the sudden change in the received signal power level. When the received signal power suddenly gets lower at 6m, the receiver would accumulate more preamble symbols. Thus, the number of preamble accumulated for the 1536 and the 2048 preamble lengths rise sharply at 6m. At 7m, the corresponding received power level rises, causing the numbers of preamble accumulated to drop. However, as distance increases, the received signal power level becomes lower again. Thus, the number of accumulated preamble symbols rises again at 8m, and stays quite constant from then on.

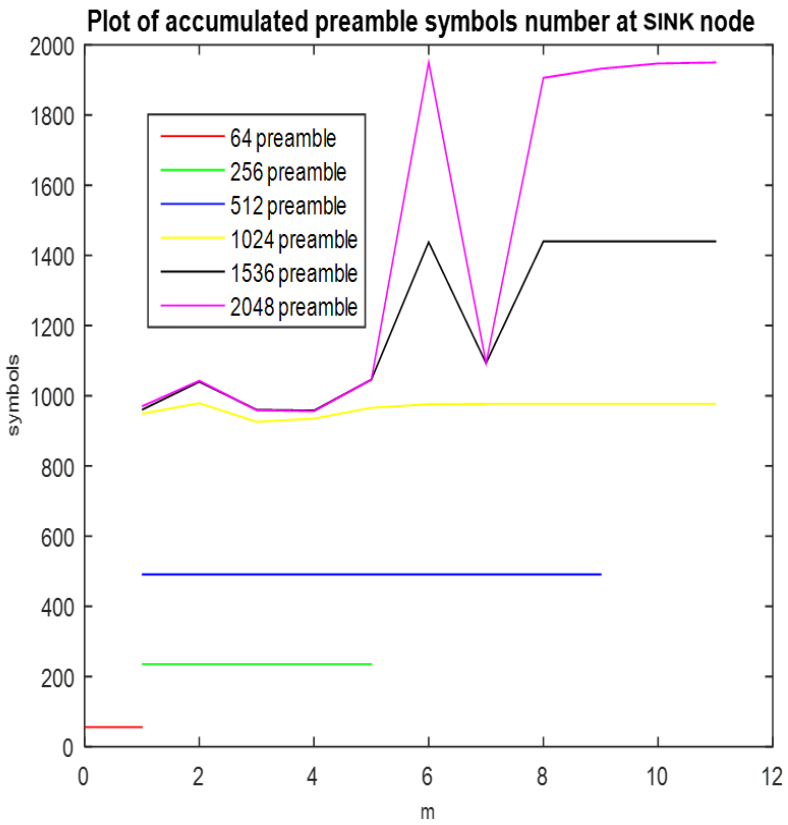

Figure 4.11. Graph of the preamble symbols accumulated at the SINK.

Fig 4.12 shows the numbers of preamble symbols being accumulated at the END. It can be seen that the same trend like that in the SINK takes place here. By comparing Fig 4.11 and Fig 4.12, we can find that there are always slightly more preamble symbols being accumulated for each preamble length in the SINK node than in the END node. This fact is quite similar to the case in the first scenario, where the SINK node has more accumulated preamble symbols than the END node at short distances. Based on previous discussion, this is caused by the END not ready to receive the ACK packets' preamble symbols, while the SINK has already begun transmitting the ACK.

Another point is that, even though the SNRs in the second scenario are much higher than those in the first scenario, the numbers of preamble symbols being accumulated in the second scenario are not necessarily larger than the number of preamble symbols being accumulated at short distances in the first scenario. This is probably because the received signal power at short distances is also sufficient in the first scenario, and there is no big difference in the number of accumulated preamble symbols.

Fig 4.13 shows the working ranges of the different preamble lengths in the perspective of the END node. It is quite noticeable that in the SINK node, there are no missing data packets for all the preamble lengths at any distance. For the 64 preamble length, the good data packets reception rate is about 98% in the SINK node. For the rest of the preamble lengths, the good data packets reception rate is 100% in the SINK. In the END node, there are occasionally FWTO errors taking place at some distances. This suggests that there are missing ACK packets. For the 64 preamble length, there are other errors except the FWTO at the END node. For the rest of the preamble lengths, there are only FWTO errors at the END node.

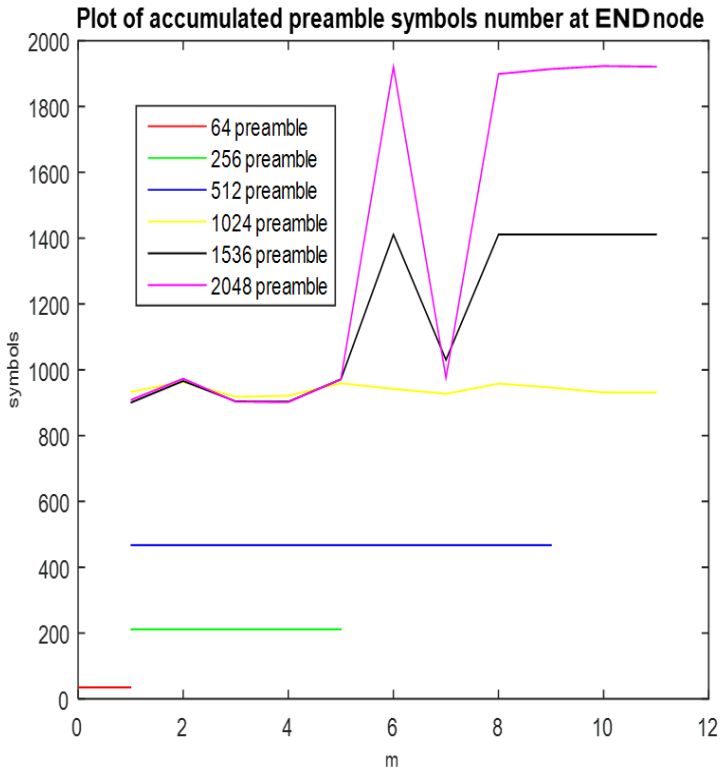

Figure 4.12. Graph of the preamble accumulated at the END.

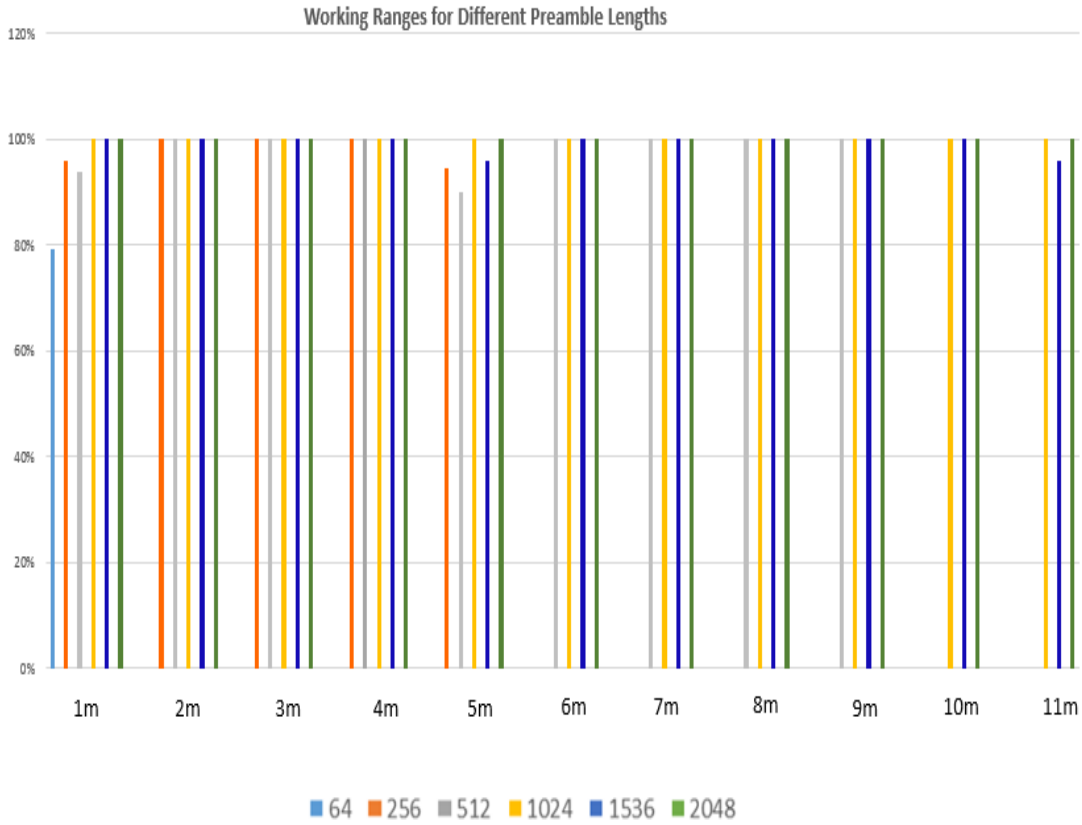

Fig 4.13. Graph of working ranges of different preamble lengths.

There is another noticeable phenomenon happening in measurements of the second scenario. Each preamble length has a working range. Within the working range, the data reception performed outstandingly, with a 100% packets reception rate at most of the time. There were occasional cases, where the packets reception rates were not 100%. However, even for those occasional cases, the packets reception rates were always above 90%. Nevertheless, when passing the working range of a preamble length, that preamble length's performance totally failed: while taking each measurement of sending the 4000 packets, the two devices would suddenly quit working in the process. This was just like in the case of a 'cold start up', where two devices were totally 'unfamiliar' with each other. Moreover, longer preambles had larger working ranges.

This result had just proven the prediction being made on the system's stability in the previous chapter. Based upon previous introduction, this was caused by too many block fading channel impulse responses taking place in the random delay between two packets.

Table 4.7. Counters of the 64 preamble length in the second scenario

	1m END	1m SINK
PHE	45.1	0.3
RSE	66.5	15.3
FCG	3177	3984
FCE	1.8	0
FFR	218.6	0.3
FWTO	491	0
TXFS	4000	3984
PreambleACC	35.1	55.7
RXlevel (dBm)	-86.8	-85

Table 4.7 shows the counters' values of the 64 preamble length. It can be seen that the 64 preamble length's overall performance in the second scenario at the END node is even worse than that in the first scenario. There are 491 FWTO errors, which suggest that the receiver fails to detect any preamble symbol. Thus, the 64 preamble length's ACK packets have synchronization problem in the second scenario.

Those 491 FWTO errors are much more than the corresponding 44 FWTO errors in the first scenario. This would suggest that the synchronization ability of the 64 preamble length's ACK packets is even worse in the second scenario than in the first scenario. However, the other errors of the 64 preamble length of the second scenario at the END node are less than those of the first scenario. Another noticeable fact of the 64 preamble length is that it has a large number of FFR errors at the END node in both the first and the second scenario.

The fact that those other errors are less should be the result of a higher SNR. The synchronization problem of the 64 preamble length's ACK packets might be caused by other unknown reasons.

5. Conclusions

This thesis studied the performance of the DW1000, which implements the PHY and some MAC specifications of IEEE 802.15.4-2011 UWB standard. More specifically, the thesis focused on finding out different preamble lengths' synchronization ability and the effects of multipath propagation on the system, through taking measurements. Various conclusions have been drawn out from the measurements' results.

The first chapter of this thesis gave an overall introduction on the entire thesis. The research questions and the motivation for the thesis were given. The approaches to solve the problems were briefly discussed.

The second chapter of this thesis introduced the basic concepts of the UWB systems and the physical structure of the IEEE 802.15.4-2011 UWB specifications. In additions, different channel models, which could be used to analyze the results, were discussed in detail. In general, chapter two provided a theoretical basis for solving the problems.

The third chapter of this thesis introduced the measurements' settings in detail. First, the DW1000's necessary functionalities and operational process, which were based on the PHY and some MAC features of the IEEE 802.15.4-2011 UWB standard, were discussed in detail. Second, both parts of the measurements' settings and steps were introduced thoroughly, so that the statistics of the results could be determined. Third, some theoretical predictions on the possible outcomes of the results were given.

The fourth chapter of this thesis provided the results of both parts of measurements. Based upon those results, analysis was made. Conclusions were drawn in order to give answers to the initial research questions.

Finally, the current chapter gives a brief review on the whole thesis Besides giving solutions to the original problems, this chapter also points out the possible future work needed to be done.

5.1. Basic concepts

The UWB system being studied, is based upon impulse radio scheme. The spreading of one bit of information over multiple UWB pulses can combat noise and interferences. In the IEEE 802.15.4-2011 UWB specifications, the BPM/BPSK modulation scheme is being used. The BPM/BPSK is the combination of the time-hopping and direct sequence schemes. The large time hopping frame provided rejection to many kinds of interferences, such as multi-user interference and inter-symbol interference (ISI). The direct sequence technique randomizes the UWB signal, and makes it more noise-like towards other communication systems.

There are various models describing the UWB channel characteristics. Unlike conventional narrow band systems, the multipath components of a UWB signal often arrive in clusters. Compared with the other channel models, the S-V model is more appropriate for describing a UWB channel. However, it may have some defects on predicting a LOS environment.

In the IEEE 802.15.4-2011 UWB specifications, a frame is consisted of five parts: the preamble part, the SFD, the physical header, the MAC header (MHR), and the data payload. The preamble part is used for synchronization, while the SFD marks the change from preamble detection and accumulation to the demodulation of the PHR, the MHR, and the data payload. The PHR contains crucial information on the

demodulation of the data payload, such as the data rate and the frame length. The address and the frame type information is included in the MHR. At the end of the data payload, there is the frame check sequence to help the receiver check whether the received information is correct or not.

The DW1000 is a low-cost and low-complexity device, and compliant with IEEE 802.15.4-2011 UWB specifications. The low complexity is due to using the ED receiver. It has the advantage of accumulating more energy in environments with multipath propagation. However, it is vulnerable to multi-user interference.

5.2. Measurements and predictions

The operational process of the devices remained constant during both parts of the measurements. At first, the END node would transmit a data packet to the SINK node. After the transmission of a data packet, the END node would transit into receiving mode for the ACK frame's reception. Meanwhile. The SINK node would make decision on whether to send the ACK or not, based on the data packet it had received. If the data packet had passed the FCS checking, the SINK node would send the ACK back.

At the END node's side, if it had received the ACK frame within a certain fixed time duration, the END node would check the ACK frame. After checking the ACK frame, the END would go on to transmit the next data packet. If the END node hadn't detected the ACK frame within the certain time duration, it would count it as a frame wait time out (FWTO) error, and go on to transmit the next data packet. Due to coding and programming issues in our measurements, the SINK node would actually transmit the ACK frame a little bit earlier than the END node could be ready to receive it.

The first part of the measurements were done in an anechoic chamber with minimum multipath reflections. The purpose was to find different preamble lengths' synchronization ability. It was expected that a longer preamble length would offer a better synchronizing ability and a longer working distance.

The second part of measurements were carried out in a corridor, which could be seen as a LOS environment. The environment was rich with multipath components, and the channel was regarded as a block fading channel.

In the second part of measurements, the SNR should be much higher than in the first part of measurements, due to the receiver accumulating energy from the multipath components of a received pulse.

The UWB S-V channel model is precise in predicting a NLOS environment. However, it may have some defect in predicting a LOS environment. According to predictions in chapter three, there might be a break point distance, where the received signal power level would decrease sharply. This is quite like the situation in a narrow band system.

Block fading would cause instability in the performance. If there were too many channel impulse response changes taking place within the duration between two packets, it would become hard for the two devices to synchronize with each other again. Longer preamble lengths could offer better synchronization, thus more robust against the instability caused by block fading.

5.3. Discoveries from the results

The synchronization ability of different preamble lengths can be seen from the results of the first parts of the measurements. First, it was found out that a longer preamble length tended to have a longer working distance. This is due to the fact that the longer preambles' synchronization ability is better at long distances. Second, it was found out that the overall performance, in the term of packet reception rate, of the long preambles was not necessarily better than that of the short preambles at short distances. The 256 preamble length turned out to have the best performance within the 5m's testing range. Third, it was found out that the 64 preamble length's performance was the worst among all the preamble lengths. This might prove that the 64 preamble length is too short for synchronization,

The results of the second parts of the measurements showed how the system would perform in an environment with multipath propagation. Moreover, environment could be regarded as LOS and block fading. First, it directly proved the IEEE 802.15.4-2011 UWB specifications could take advantage of multipath propagation. Second, the sharp drop in the received signal's power level proved the fact that the UWB S-V channel model might not precisely predict the behavior of a UWB system in a LOS environment. Third, it was found out that different preamble lengths had their stable working ranges. A longer preamble length tended to have a longer stable working range. The instability of the channel was probably caused by block fading, and it would lead to synchronization problem. Fourth, the 64 preamble length did not work properly in terms of both the overall performance and the stability.

5.4. Overview on future works

This thesis pointed out that in block fading channels, the system might suffer from instability in performance. This point of view still needs to be proved by further studies. It is of great interest on finding out how to measure this instability, and prevent it from happening. Based upon previous discussion, the ED receiver is vulnerable to MUI. Thus, it is also necessary to study the performance of the system under multi-user interference.

6. References

[1] Oppermann I., Hämäläinen M. & Iinatti J. (2004) Introduction. UWB Theory and Applications, Oulu, p.1-8.

[2] Alegre Perez J.P., Celma S. & Lopez B.C. (2011) AGC Fundamentals. Automatic Gain Control Techniques and Architectures for RF Receivers, p.13-28.

[3] Oppermann I., Hämäläinen M. & Iinatti J. (2004) UWB Channel Models. UWB Theory and Applications, Oulu, p.9-38.

[4] Oppermann I., Hämäläinen M. & Iinatti J. (2004) Modulation Schemes. UWB Theory and Applications, p.39-66.

[5] UWB PHY. IEEE 802.15.4-2011. IEEE Standard for Local and metropolitan area networks. IEEE Computer Society Sponsored by the LAN/MAN Standards Committee, p.194-222.

[6] MAC Protocol. IEEE 802.15.4-2011. IEEE Standard for Local and metropolitan area networks. IEEE Computer Society Sponsored by the LAN/MAN Standards Committee, p.18-76.

[7] DW1000 Data sheet, 44p.

[8] Overview of the DW1000. DW1000 User Manual, p.9-23.

[9] Message Transmission. DW1000 User Manual, p.23-29.

[10] Message Reception. DW1000 User Manual, p.29-44.

[11] Media Access Control (MAC) Hardware Features. DW1000 User Manual, p.45-50.

[12] Other Features of the DW1000. DW1000 User Manual, p.51-58.

[13] The DW1000 Register Set. DW1000 User Manual, p.59-184.

[14] Operational Design Choices When Employing the DW1000. DW1000 User Manual, p.193-198.

[15] Chu X. & Ross D.M. (2004) The Effect of NBI on UWB Time-Hopping Systems. IEEE Transactions on Wireless Communications, Vol.3, p.1431-1436.

[16] Niemelä V., Haapola J., Hämäläinen M. & Iinatti J. (2012) Integration Interval and Threshold Evaluation for An Energy Detector Receiver with PPM and OOK Modulations. In: Proceedings of the 7th International Conference on Body Area Network, September 24-26, Oslo, Norway.

[17] Hämäläinen M. & Iinatti J. (2005) Interference and Distance Studies for DS-UWB. University of Oulu, Center for Wireless Communications (CWC), Oulu.

[18] Flury M., Merz R. & Boudec J.L. (2011) Synchronization for Impulse – Radio UWB with Energy-Detection and Multi-User Interference: Algorithms and Application to IEEE 802.15.4a. IEEE Transactions on Signal Processing, Vol.59, p.5458-5472.

[19] Dwan C., Orlik P., Sahinnoglu Z. & Molish A.F. (2007) A Non-Coherent 802.15.4a UWB Impulse Radio. In: Ultra-Wideband, 2007. ICUWB 2007. IEEE International Conference on, September 24-26, Singapore, p.146-151.

[20] Stoica L. (2008) Non-coherent Energy Detection Transceivers for Ultra Wideband Impulse Radio Systems. Public Defense, Paahensali, Linnanmaa, Oulu, 161p.

[21] Lievenoogen B.V. (2008) Investigation of the suitability of Ultra Wideband in military scenarios. Delft University of Technology, Mathematics and Computer Science, Delft.

[22] IR_001: UWB performance experiment (2015) CWC, Oulu, 18p.

[23] He N.& Tepedelenlioglu C. (2006) Performance Analysis of Non-Coherent UWB Receivers at Different Synchronization Levels. IEEE Transactions on Wireless Communications, Vol.5, p.1266-1273.

[24] Linnartz J.P. & Davis J.S. (1997) Indoor Wireless RF Channels. URL: http://www.wirelesscommunication.nl/reference/chaptr03/indoor.htm.

[25] PanOulu Equipment. URL: https://www.panoulu.net/wsn/equipment.

[26] PanOulu Access Point List. URL; https://www.panoulu.net/wlan/ap.

[27] Materials-Light and Reflecting Factor. URL: http://www.engineeringtoolbox.com/light-material-reflecting-factor_1842.html.

[28] eduroam. URL: https:// www.eduroam.org/.

[29] Sato S. & Kobayashi T. (2004) Path-loss exponents of ultra wideband signals in line-of-sight environments. In: Spread Spectrum Techniques and Applications, 2004 IEEE Eighth International Symposium on, August 30-September 2, p.488-492.

[30] Aroonpraparat S., Supanakoon P., Promwong S. & Takada J.I. (2006) Path Loss Expressions of Ultra Wideband Ground Reflection Channel. In: Communications and Information Technologies, 2006. ISCIT '06. International Symposium on, October 18- September 20, Bangkok, p.1017-1020.

[31] Andreas F.M., Kannan B., Dajana C., Chia C.C., Schahriar E., Andrew F., Johan K., Juergen K., Hans S., Ulrich S., & Kai S. (2004) IEEE 802.15.4a channel model-final report. IEEE 802.15.4a channel modeling subgroup, 40p.

[32] Siriwongpairat W.P., Su W. & Liu K.J.R. (2006) Performance characterization of multiband UWB communication systems using Poisson cluster arriving fading paths: Selected Areas in Communications, IEEE Journal on, Vol.24, p.745-751.

[33] Yanjing S. & Li p. (2009) the Simulation and Analysis of UWB Modified S-V Channel Model. In: Wireless Communications, Networking and Mobile Computing, 2009. WiCom '09. 5th International Conference on, September 24-26, Beijing, p.1-4.

[34] Benedetto M.G.D., Kaiser T., Molish A.F., Oppermann I., Politano C. & Porcino D. (2006) UWB Communication Systems: A Comprehensive Overview. EURASIP Signal Processing and Communications, 497p.

[35] Yuce M.R. (2013) Ultra-Wideband and 60 GHz Communications for Biomedical Applications. Electrical and Computer Systems Engineering, Clayton, 254p.

[36] Thotahewa K.M.S., Redoute J.M. & Yuce M.R. (2014) Ultra Wideband Wireless Body Area Networks. Electrical and Computer Systems Engineering, Melbourne, 170p.

[37] Nekoogar F. & Dowla F. (2012) Ultra-Wideband Radio Frequency Identification Systems. Lawrence Livermore National Laboratory, Livermore, 172p.

[38] Emami S. (2013) UWB Communications Systems: Conventional and 60 GHz, Principles, Design, and Standards. Samsung R&D, San Jose, 235p.

[39] Wu D., Bao L. & Li R. (2009) UWB-Based Localization in Wireless Sensor Networks. International Journal of Communications, Network and System Sciences, Vol.2, p.407-421.

[40] Pancera E. (2010) Medical applications of the Ultra Wideband technology. In: Antennas and Propagation Conference (LAPC), November 8-9, Loughborough, UK, p.52-56.

[41] Kidera S., Sato T. & Sakamoto T. (2010) Accurate UWB Radar Three-Dimensional Imaging Algorithm for a Complex Boundary Without Range Point Connections. Geoscience and remote sensing, IEEE Transaction on, Vol.48, p.1993-2004.

[42] Salman R. & Willms I. (2011) 3D UWB radar super-resolution imaging for complex objects with discontinuous wavefronts. In: Ultra-Wideband (ICUWB), IEEE International Conference on, September 14-16, Bologna, Italy, p.346-350.

[43] Yarovoy A.G., Savelyev T.G., Aubry P.J., Lys P.E. & Ligthart L.P. (2007) UWB Array-Based Sensor for Near-Field Imaging. Microwave Theory and Techniques, IEEE Transactions on, Vol.55, p.1288-1295.

[44] Zwirello L., Schipper T., Jalilvand M. & Zwick T. (2014) Realization Limits of Impulse-Based Localization System for Large-scale Indoor Applications. Instrumentation and Measurement, IEEE Transactions on, Vol.64, p.39-51.

[45] Hazra R. & Tyagi A. (2014) A Survey on Various Coherent and Non-coherent IR-UWB Receivers. India Institute of Technology, Department of Electronics and Communication Engineering, Roorkee.

7. Appendices

Appendix 1. END Node's FWTO values of different preambles in second scenario

	1m	5m	11m
256	155	222	-
512	254	403	-
1536	0	155	150